Project ATLAS Hybrid Rocket Engine

Final Thesis Report

A Technical Report submitted to the Department of Aerospace and Mechanical Engineering

Presented to the Faculty of the School of Engineering and Applied Science

University of Virginia • Charlottesville, Virginia

In Partial Fulfillment of the Requirements for the Degree

Bachelor of Science, School of Engineering

Harshit Dhayal

Spring 2025

Capstone Project Team Members

Gavin Miller, Ved Thakare, Mannix Green, Aiden Winfield, Sean Dunn, Dominic Profaci, Thomas DeCanio, Joshua Bird, Harrison Bobbitt, Taka Suzuki, Darsh Devkar, Jack Spinnanger, Isaac Tisinger, Silas Agnew, Zach Hinz, Alexander Gorodchanin, Adis Gorenca, James Dalzell

On my honor as a University Student, I have neither given nor received unauthorized aid on this assignment as defined by the Honor Guidelines for Thesis-Related Assignments

Dr. Chloe Dedic, Department of Mechanical and Aerospace Engineering

Dr. Daniel Quinn, Department of Mechanical and Aerospace Engineering

Contents

1 Variable List

A^*	Area of the Nozzle Throat (m^2)
A_e	Area of the Nozzle Exit (m^2)
c^*	Characteristic Velocity (m/s)
c_e	Effective Exhaust Velocity (m/s)
c_F	Thrust Coefficient
F_{avg}	Average Thrust (N)
g	Acceleration Due to Earth's Gravity (m/s^2)
I_{sp}	Specific Impulse (s)
M_e	Nozzle Exit Mach Number
M^*	Nozzle Throat Mach Number
$\dot{m}_{noz}$	Mass Flow Rate at the Nozzle (kg/s)
O/F	Oxidizer to Fuel Ratio
p_a	Ambient/Back Pressure (Pa)
p_c	Chamber Pressure (Pa)
p_e	Nozzle Exit Pressure (Pa)
p^*	Nozzle Throat Pressure (Pa)
R_c	Specific Combustion Gas Constant $(J/(kg \cdot K))$
T_c	Chamber Temperature (K)
T_e	Nozzle Exit Temperature (K)
T^*	Nozzle Throat Temperature (K)
v_e	Exhaust Velocity (m/s)
Δt	Total Burn Time (s)
γ	Ratio of Specific Heats, Combustion Gas
Γ	Isentropic Constant, Combustion Gas
ϵ	Expansion Ratio

2 Abstract

An H-class hybrid rocket engine (Fig: 1) was developed for static testing of additively manufactured performance-enhancing components. The engine was designed for multiphase oxidizer and 3D-printed solid fuel grain propellants. A complete modular test stand with blast shields was designed to support a static testing campaign. This test stand supported an oxidizer supply system and data acquisition and control test for accurate data collection during tests. The engine was then tested through hydrostatic, cold flow, and hot fire test campaigns.

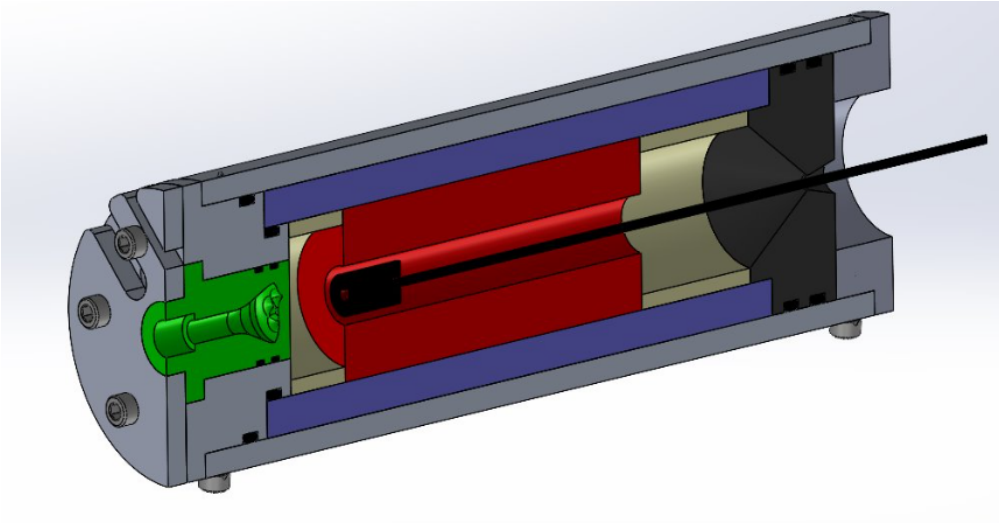

Figure 1: Section view of ATLAS hybrid rocket engine.

3 Introduction

Hybrid rocket engines are the standard for student-researched and developed (SRAD) rocketry projects due to their safety, simplicity, and high performance. These engines are propelled by a combusting mixture of solid fuel and liquid or gaseous oxidizer. The fuel is stored within the combustion chamber in the form of a grain. The oxidizer is injected into the chamber from an external storage system. While the solid fuel greatly simplifies the engine system and prevents thermal runaway during combustion and while the oxidizer systems allows for easy throttling of the flow, hybrid engines are not without their disadvantages. Hybrid engines are scalable to a limit. Large hybrid engines do not provide adequate surface area to burn their large volumes of fuel

grain quickly enough to achieve launch velocities high enough for liftoff. This concern was realized early on in the development of hybrid engines, but is of little concern as medium- and heavy-class liquid engines are so well-developed. The constraint simply compartmentalizes hybrid engines for use on small launch vehicles and by student teams, already their primary users. Additionally, the hybrid engine combustion process, driven by fuel regression rates and oxidizer/fuel boundary layer effects, is extremely difficult to model and often must be tested to verify performance. Even then, performance varies throughout the burn as a result of changing grain geometries and fluctuating oxidizer mass flow rates. Empirical data for regression rates are limited, and systems that stabilize thrust production are often complex and difficult to manufacture. These systems can implement metal 3D-printed injection systems for optimal performance, a resource that is usually out of reach of small companies and student-led teams.

Aerospace Engineering Capstone Team 3 at the University of Virginia (UVA), composed of 19 students, developed the ATLAS hybrid rocket engine to make progress toward better characterizing the performance of hybrids, at low cost. The engine and supporting test stand were developed as a testbed for examining the effects of fuel grain geometry and injector design on performance. Fifteen different fuel grain geometries were designed for performance testing, as well as three different ignition systems. The injection systems were 3D-printed using high-temperature resistant resin, a design entirely unique within the hybrid community which allows for optimized geometries at extremely low cost and difficulty in manufacturing. The test stand, depicted in Fig. 2, ensures the engine is structurally stable during testing. It is remotely operable and capable of gathering thrust, temperature, pressure, and infrared video feed data thanks to its data acquisition (DAQ) and control system. Project ATLAS was also developed to lay the groundwork for future SRAD engine projects at UVA. The safety and test procedures for this engine can easily be carried over to future projects, and much of the test data from ATLAS can be used to improve the design and predict the performance of the UVA Rocketry Team's competition engine, PROMETHEUS.

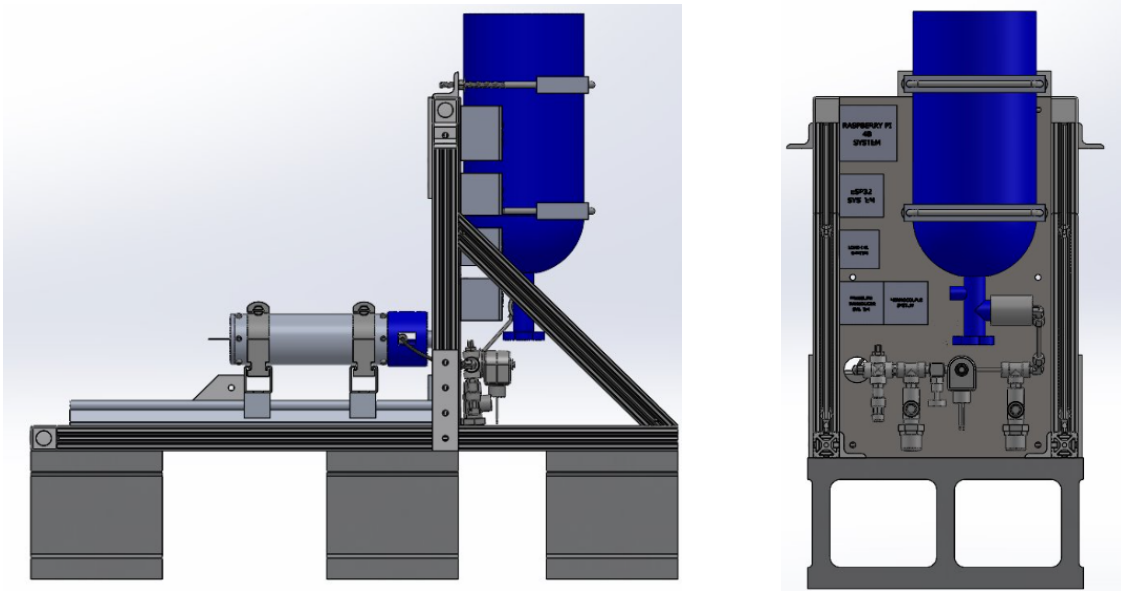

(a) Side view of test stand.

(b) Rear view of test stand.

Figure 2: Test stand system with ATLAS engine, plumbing, and control boxes mounted.

4 System Assembly

The team elected to break the engine down into four major subsystems, each of which was developed separately by an individual team. These systems are: combustion devices subsystem, oxidizer supply system, pyrotechnics subsystem, and ground testing subsystem. A layout of the different systems can be seen in Fig. 3.

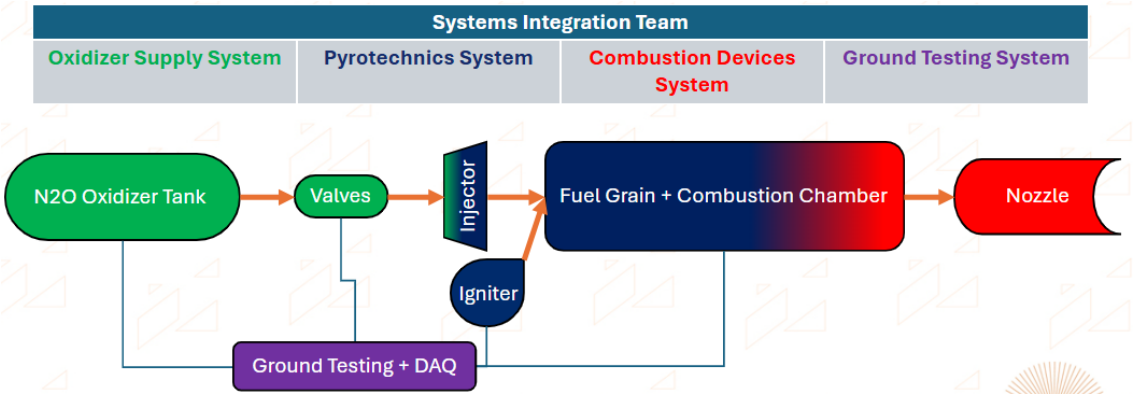

Figure 3: Breakdown of major project systems.

The combustion devices system is the engine proper. It consists of the combustion chamber, nozzle, thermal protection system, engine bulkheads, and sealing system. An H-class engine, storing 160-320 N-s of total impulse, was chosen for the ATLAS design as it is operable by an

individual with a Tripoli L1 certification and is small enough to minimize risk while still producing interesting operating conditions. ATLAS was designed to achieve the high end of this range, close to 320 N-s.

The combustion chamber was designed to sustain combustion, house the fuel grain, seal during operation, and withstand design pressure and temperature of 500 psi and 3300 K, respectively. The nozzle must accelerate the flow to supersonic speeds, maximizing thrust production. In addition, the engine must fire for at least 5 seconds at a time. This greatly influences the design of the engine and nozzle. Most H-class hybrid engines burn for only 0.5-1 seconds at a time and produce high thrust. Because longer burn times are desired for ATLAS so that more performance data can be gathered and the results more easily extrapolated to larger engines such as PROMETHEUS, the engine was designed to produce low thrust for longer periods of time. The combustion devices system is described in great detail in section 5.

The oxidizer supply system consists of the external oxidizer storage tank, a control valve, a throttling valve, plumbing lines, fittings, and the injection system. Its primary role is to supply oxidizer at a high pressure and steady mass flow rate to the engine for combustion. The injection system must atomize the oxidizer flowing, essentially converting multi-phase or liquid oxidizer into a gas that can then be easily mixed with the pyrolyzed fuel grain boundary layer for combustion. Nitrous oxide (N2O) was chosen as the oxidizer as it is easy and safe to store and transport and allows for a greatly simplified self-pressurized oxidizer supply system design. The injection and oxidizer supply subsystem is described in section 6.

The pyrotechnics system is composed of the fuel grain and the ignition system. This subsystem is responsible for initiating and sustaining combustion. The fuel grain must provide enough mass for sustained combustion throughout the desired burn duration. Additionally, it must incorporate a port geometry that is condusive to easy starting and burning and promotes consistent or controllable regression throughout the course of the burn. These qualities are difficult to predict and characterize, thus 15 fuel grains were designed for testing. The fuel chosen was ABS plastic as it is inexpensive and can be 3D-printed. 3D-printing allows for maximum flexibility in design and manufacturing, while simultaneously avoiding difficult vacuum casting fuel grain manufacturing

methods. The ignition system must create a sustained flame that is hot enough to pyrolyze the fuel grain and decompose the N2O into N2 and O2. The N2 is ejected to produce momentum thrust and the O2 reacts with the fuel grain. Several different ignition systems were designed and tested. The details of these subsystems are given in section 7.

The ground testing system was broken down into two components: structural and DAQ/control. The structural subsystem must stabilize the rocket during firing, ensuring a completely static test. It must also contain debris and shield operators and sensitive components in all but the exhaust stream direction in the event of a destructive test. The DAQ/control system must control the valves and ignition system, monitor live temperature, pressure, and thrust data, and stream live video feed during the test. It must allow for remote control of all systems, as well as remote initiation and shutdown of the ignition sequence. The details of this system are given in section 8.

Each system team consisted of 4-5 members and was led by a team leader. The test stand system had a structural lead and DAQ lead due to the size and complexity of the system. The system-level teams were overseen by the leadership team, the members of which functioned as systems engineers. Each member of the leadership team also had an individual role on one of the system-level teams. After the design and analysis phase, the system teams disbanded to help wherever needed during the manufacturing and test phases. The leadership team maintained its structure and assisted wherever needed. The details of the team structure are given in Appendix A.

The ATLAS Project was funded $200 per student and $750 from the faculty advisors, totaling $4550. Appendix B details an itemized list of all purchases by each sub-team. The capstone team was able to successfully conduct its experiments using $3800 of the total $4550.

5 Combustion Devices Subsystem

5.1 Chamber Structure

The design of the combustion chamber structure began with a known internal pressure requirement. Using this pressure, the hoop and longitudinal stresses were calculated based on standard thick-

walled pressure vessel theory [Momot, M, 2023]. The hoop stress was determined using,

$$\sigma_{\theta\theta} = \frac{p_i a^4 - p_o b^2 a^2 - a^2 b^2 (p_o - p_i)}{a^2 (b^2 - a^2)} \tag{1}$$

where p_i and p_o are the internal and external pressures, and a and b are the inner and outer radii, respectively. We used a script to calculate the safety factor for different thicknesses given a set outer diameter. We assumed that due to thermal factors the allowable stress would be 80% of what it would be otherwise and that we would consider yielding to be failure. We did not take into account fatigue. Ultimately we decided on 0.25 inches thickness for the walls as it achieved a high factor of safety of 6.65 while being readily available for purchase.

5.2 Thermal Insulation

Phenolic was selected for the chamber lining based on availability. Two phenolic components were designed: a base liner and an internal phenolic assembly to create pre-combustion and post-combustion chambers. A fuel grain positioned between these spacers allowed for intermediate mixing zones.

Based on tests conducted by another rocketry team, phenolic liner ablation was found to be very small, and a thickness of 0.215 inches was found to be suitable for their purposes [Dundas et al., 2018]. Thus, we chose a thickness of 0.375 inches as it was commercially available and well above the necessary thickness given by the first order approxmation for hoop stress. The outer diameter of the phenolic liner set the inner diameter of the aluminum combustion chamber tube. A commercially available aluminum tube with an outer diameter of 3.5 in. and an inner diameter of 2.5 in. was selected. The concentric layers are depicted in Fig. 4. It should be noted that for rockets of this size, phenolic liner is typically unavailable as it is unnecessary due to low firing times. The chamber was sized according to the available phenolic liner, needed due to the longer firing times. All other dimensions were driven by the size of the phenolic liner, leading to the high safety factors.

Due to our aforementioned high factor of safety in the chamber wall as well as the thickness of the phenolic liner and brief duration of heating it was predicted that thermal stress would be

acceptable.

O-rings were selected based on the Titan II design decisions and gland sizing tables from Half-Cat Rocketry [Pentagon Turbot, nd, Perez et al., 2022]. Due to the lower power of our motor compared to Titan II and lack of stringent mass constraints, the same O-rings could be used, resulting in a high factor of safety. The same O-rings were used for the nozzle interface to ensure sealing effectiveness and reduce part count.

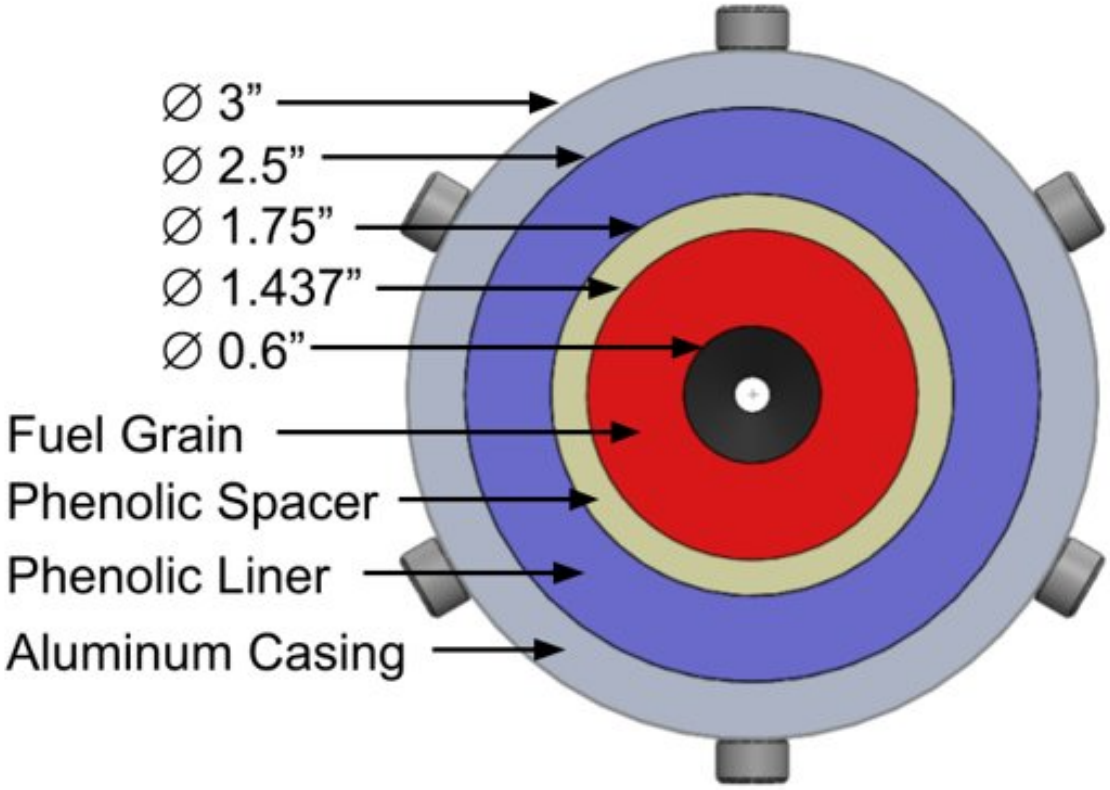

Figure 4: Section view of combustion chamber with dimensions in inches.

5.3 Nozzle

The nozzle design was based on several simplifying assumptions:

- Perfect expansion to ambient ($p_e = p_a$), eliminating pressure thrust.
- Adiabatic, frictionless, and reversible flow, permitting use of isentropic flow equations.

From the specific impulse I_{sp}, the effective exhaust velocity c_e and nozzle mass flow rate $\dot{m}_{noz}$ were calculated:

$$c_e = I_{sp} g \tag{2}$$

$$\dot{m}_{noz} = \frac{F_{avg}}{c_e} \tag{3}$$

Since $p_e = p_a$, the effective exhaust velocity simplifies to:

$$c_e = v_e \tag{4}$$

Plugging in values yielded $c_e = v_e = 2280.8$ m/s and $\dot{m}_{noz} = 0.02806$ kg/s.

Assuming the combustion chamber gas is stagnant, the exit Mach number M_e was calculated:

$$M_e = \sqrt{\frac{2}{\gamma - 1}\left[\left(\frac{p_c}{p_e}\right)^{\frac{\gamma-1}{\gamma}} - 1\right]} \tag{5}$$

The nozzle expansion ratio ϵ followed:

$$\epsilon = \frac{A_e}{A^*} = \left(\frac{1}{M_e}\right)\sqrt{\left[\left(\frac{2}{\gamma+1}\right)\left(1 + \left(\frac{\gamma-1}{2}\right)M_e^2\right)\right]^{\frac{\gamma+1}{\gamma-1}}} \tag{6}$$

Using empirically estimated properties for nitrous oxide and ABS combustion products ($\gamma = 1.257$, $R_c = 320$ J/(kg $\cdot$ K)) [Newlands, 2017], the following results were obtained:

$$M_e = 2.880, \quad \epsilon = 4.940$$

$$T_c = 3220 \text{ K}, \quad T^* = 2850 \text{ K}, \quad T_e = 1560 \text{ K}, \quad p^* = 1.910 \text{ MPa}$$

The characteristic velocity c^* and thrust coefficient c_F were computed:

$$c^* = \sqrt{\frac{R_c T_c}{\Gamma}} \tag{7}$$

$$c_F = \sqrt{\Gamma\left(\frac{2\gamma}{\gamma-1}\right)\left(1 - \left(\frac{p_e}{p_c}\right)^{\frac{\gamma-1}{\gamma}}\right)} \tag{8}$$

where $\Gamma = \left(\frac{2}{\gamma+1}\right)^{\frac{\gamma+1}{\gamma-1}}$.

Results:

$$c^* = 1539.8 \text{ m/s}, \quad c_F = 1.48$$

The relationship $c_e = c^* c_F$ was verified.

The throat area A^* and exit area A_e were then calculated:

$$A^* = \frac{\dot{m}_{noz} c^*}{p_c} \tag{9}$$

$$A^* = 1.25 \times 10^{-5} \text{ m}^2, \quad A_e = 6.19 \times 10^{-5} \text{ m}^2$$

A 15-degree full-length conical nozzle was selected for simplicity and manufacturability, offering a theoretical 98% efficiency relative to the isentropic, ideal nozzle [Sutton and Biblarz, 2017]. A section view of the nozzle is depicted in Fig. 5. The nozzle length L_t can be calculated by:

$$L_t = \frac{r_e - r^*}{\tan(\theta/2)} \tag{10}$$

where r_e and r^* are the radii at the exit and throat, and θ is the full cone angle.

5.4 Analysis

Analytical performance calculations were critically verified by utilizing the NASA tool Chemical Equilibrium with Applications (CEA) through the python wrapper RocketCEA. A script was developed to run the tool using our non-standard propellant combination of Acrylonitrile Butadiene Styrene (ABS) plastic and liquid nitrous oxide. The assumptions of Frozen Flow and Infinite-Area Combustion chamber (IAC) were determined to best suit our design. CEA was run over a range of O/F ratios and chamber pressures to produce Fig. 6. This revealed that I_{sp} can be maximized to 236.4 seconds at our design operating pressure with an O/F ratio of 5, dictating our oxidizer mass flow rate. CEA results also produced more accurate values for various parameters at select

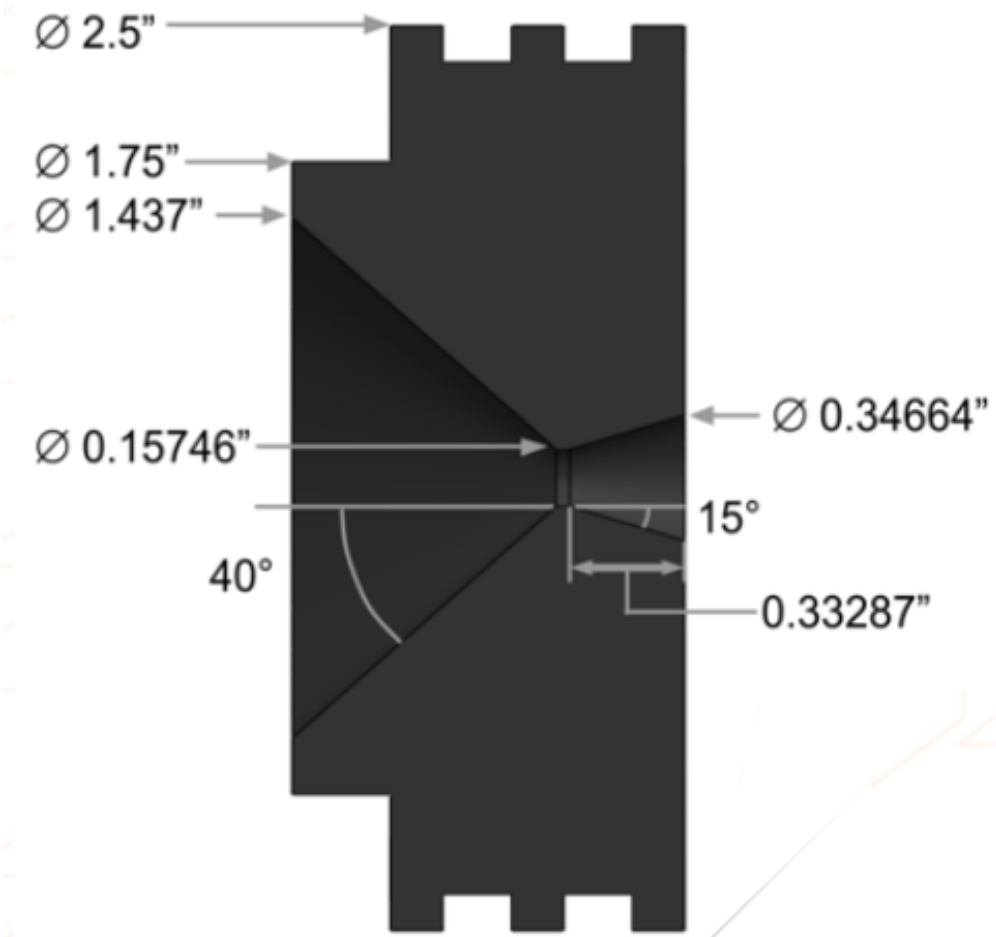

Figure 5: Nozzle section view with dimensions in inches.

points along the motor.

A static-structural finite element analysis (FEA) was conducted on the full chamber assembly to verify the strength of the structure at operational pressures. A quadratic order mesh was generated with various local mesh sizing and refinement adjustments. Contact between each solid body was simulated with a mix of the frictional and frictionless contact types. Surfaces which violated the small-sliding assumption were remedied by setting a Normal Lagrange contact formulation. Under the max expected pressure of 1000 psi (twice normal operating pressure), a minimum factor of safety of 1.3 was found at a small number of stress concentrators such as certain bolt holes surfaces. With the surrounding regions displaying significantly higher factors of safety, as illustrated in Fig. 7a, the design was deemed acceptable. One point of concern was the strength of the brittle ceramic-resin injector, however, this simulation reports an acceptable minimum factor

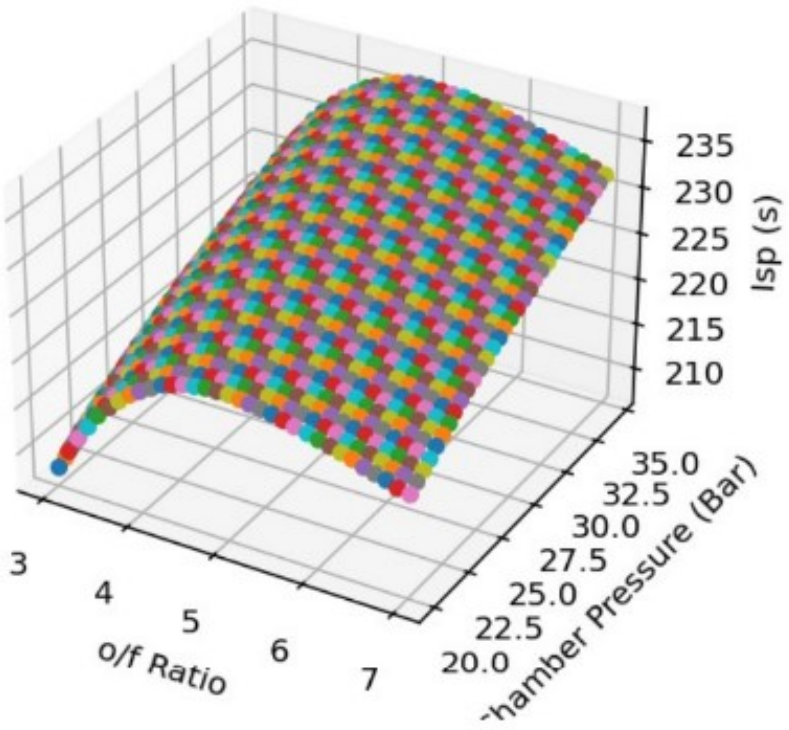

Figure 6: Isp vs Chamber Pressure vs O/F Ratio at constant expansion. Ratio

of safety of 2.37, as indicated in Fig. 7b.

A steady-state thermal and transient thermal FEA was conducted on the full chamber assembly to verify the survival of the structure at operational temperatures. To combat the persistent problem of thermal undershooting by ANSYS Mechanical, a linear order mesh was generated with a very high mesh density at surfaces with an extreme thermal gradient. Contact between each solid body was simulated with the bonded contact type. Surfaces which were over-constrained by the setup were remedied by setting an Augmented Lagrange contact formulation. All other surfaces being dictated by the Multi-Point Constraint (MPC) contact formulation to ensure no gaps were incorrectly interpreted between layers. The simulation was run under the expected operational chamber gas temperature of 3328.3 K with a convection coefficient of 7129.8 $W/m^2 * K$ applied to all surfaces as our best approximation. It was found that the low thermal conductivity of the phenolic liners and ceramic-resin injector completely protect most of the aluminum structure, as seen in Fig. 8a. As expected, the bulky aluminum forward bulkhead was able to heat sink much of the heat it received from its surface exposed to combustion gases; however, it was found that

it still reached a few hundred kelvin over its melting temperature for 4 out of 5 seconds of burn time, as evident in Fig. 8b. This prompted a design change in which a phenolic plate was added between the forward bulkhead and pre-mixing chamber phenolic spacer.

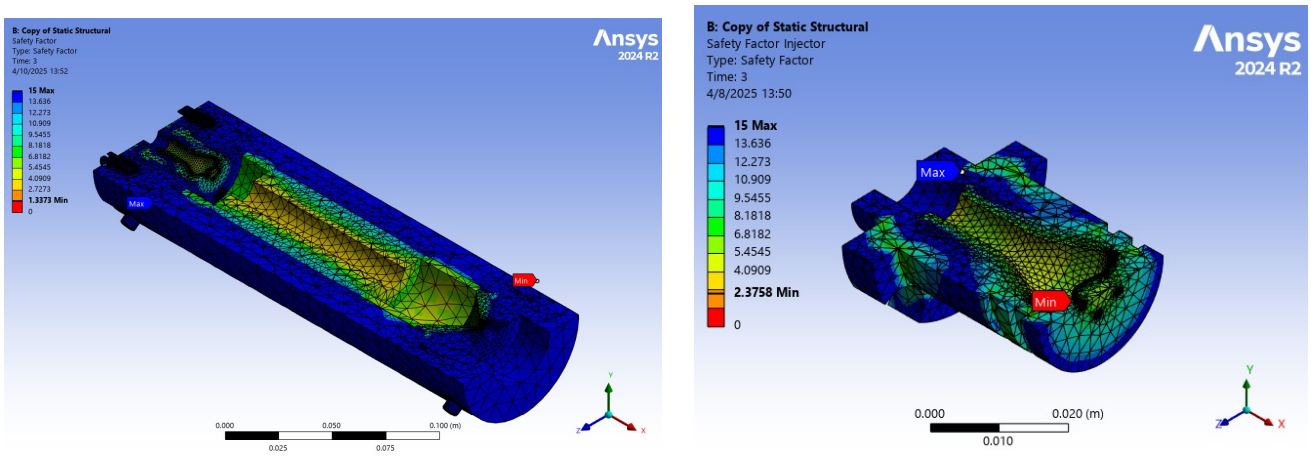

(a) Full Assembly (b) Shower-head Injector

Figure 7: Static structural FEA of the combustion chamber assembly (a) and injector (b).

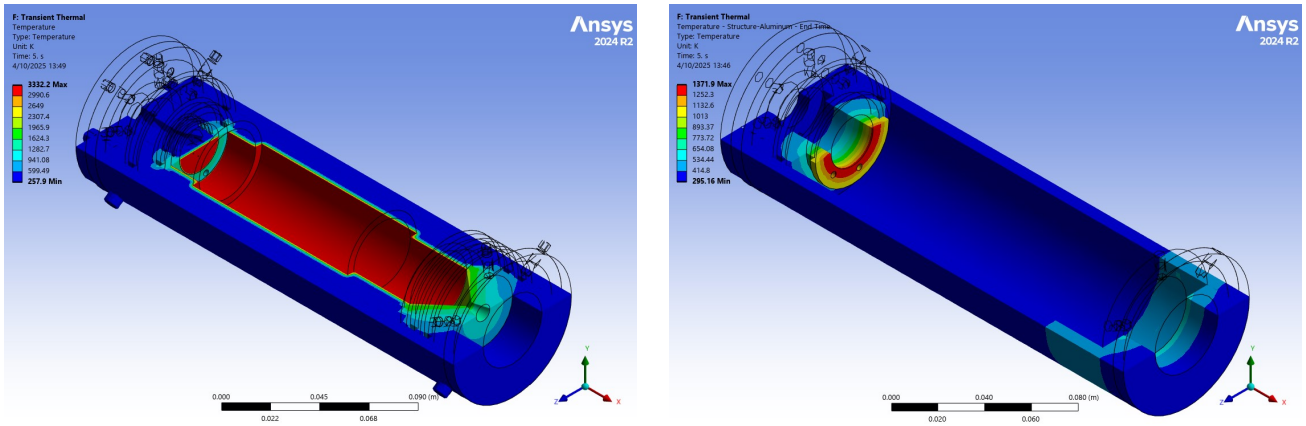

(a) Full Assembly (b) Structure

Figure 8: Transient thermal FEA of the combustion chamber assembly.

6 Oxidizer Supply Subsystem

6.1 Subsystem Overview

The primary purpose of the oxidizer subsystem is to provide the motor combustor with the flow of nitrous oxide. In order to meet the functional and operational requirements, the subsystem was

designed as in Figs. 9 and 10, in which the P&I diagram and the CAD of the system assembly are shown. More details of the subsystem are explained in the following sections.

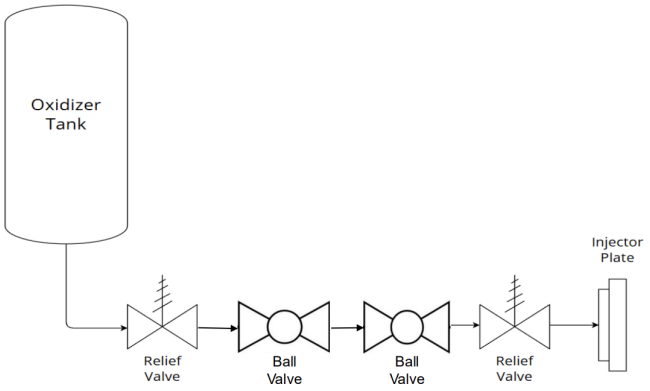

Figure 9: Oxidizer subsystem P&I diagram.

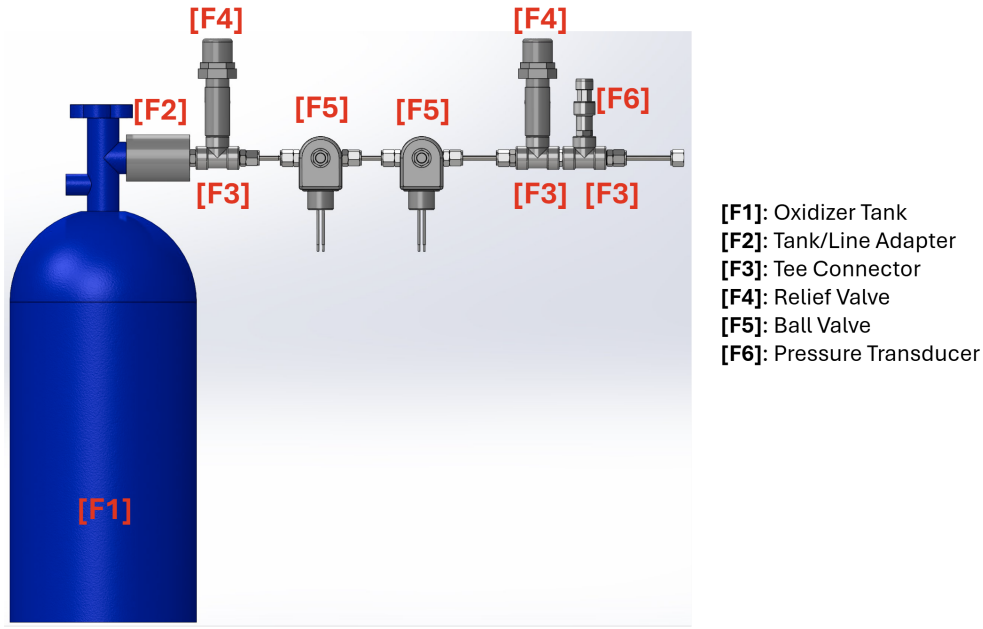

Figure 10: Oxidizer subsystem assembly CAD. Note that this view depicts all components for easy viewing, and is not representative of the plumbing arrangement in the actual assembly.

6.2 Pressure Drop

The calculated static pressure of the flow across the feed line is shown in Fig. 11. The pressure starts at 670 psi at the most upstream of the line, the exit of the tank. There is a total minor loss of 14.9 psi from the valves, tee connections, and bend along the line until the flow reaches the

injector. Across the injector, the pressure drops by 156 psi to 500 psi, the operating pressure of the combustion chamber. The calculations of major and minor losses are presented in Appendix E. Some of the K_l values used in calculations were verified with CFD in Ansys.

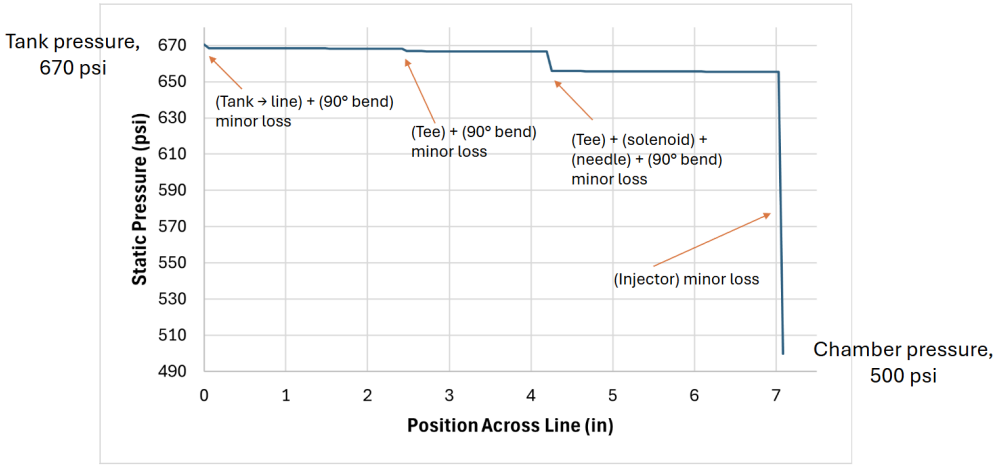

Figure 11: Theoretical static pressure of the oxidizer across the plumbing line.

6.3 Injector

Three different styles of injector were designed: showerhead, uniaxial swirl, and impinging jet, each of which was to be printed with high-temperature resin. The CAD for each is shown in Fig. 13. The function of all the injectors is the same, to vaporize the oxidizer through the pressure drop across, but different designs are intended to achieve different flow characteristics of the atomized oxidizer downstream. While the showerhead injector yields a straight, longitudinal flow, the uniaxial swirl injector aims to generate a swirling stream. The impinging jet works by leading three sets of two thin streams to collide into each other to facilitate atomization.

The uniaxial swirl and impinging jet injectors were designed to work in conjunction with the oxidizer throttling valve to produce the necessary pressure drop, so they were designed with orifices large enough to ensure the pressure drop across was not so large as to limit the required mass flow rate into the engine. The showerhead injector was designed to meet the injector pressure drop of 165 psi required in Fig. 11. This involved solving the equation for mass flow across orifices,

$$\dot{m} = C_d A n \sqrt{2 \Delta P \rho_{ox}},$$

where A is the orifice area, ΔP is the pressure drop across the injector, ρ_{ox} is the density of the oxidizer, n is the number of injector orifices, and C_d is the discharge coefficient of the injector. This coefficient was found using a formula for multi-phase flow empirically developed by Yang [Yang, 2015]:

$$C_d = 0.5542 + 0.5626\beta - 1.652\beta^2 + 1.680\beta^3,$$

where β is the ratio of orifice diameter to combustion chamber diameter. These two equations were iteratively solved using a MATLAB script which generated the plot shown in Fig. 12. The number of holes was then chosen to be 5 with a diameter of 0.5 mm due to available drill bit sizes and packaging/manufacturing limitations. An aluminum showerhead injector with four larger orifices was also developed as a backup in the event that the plastic injectors cannot withstand operational thermal loads. All injectors, including the showerheads, can be coordinated with the throttle control valve to optimize the total pressure drop across the oxidizer supply system.

A series of preliminary molecular dynamics simulations of the atomization of N2O was performed, and the results are reported in a separate document.

Injectors were manufactured using a Formlabs 3 stereolithography (SLA) printer. This allowed for complex geometries that were impossible to create with traditional manufacturing while also printing with finer accuracy compared to fused deposition modeling (FDM) printers. Additionally, this technique was utilized because parts produced using SLA printers are inherently waterproof and capable of carrying fluids, unlike parts created using FDM printers. After printing, each of the injectors was washed in isopropyl alcohol, the supports were carefully removed, and the parts were cured. This curing process was carried out in two steps: first with UV light and heat in the Form Cure post-processing station at 80 degrees Celsius for 120 minutes, then further cured in a kiln at 160 degrees Celsius for 180 minutes. This process improved the mechanical properties and heat resistance of the injectors, allowing them to survive the conditions predicted within the engine during operation.

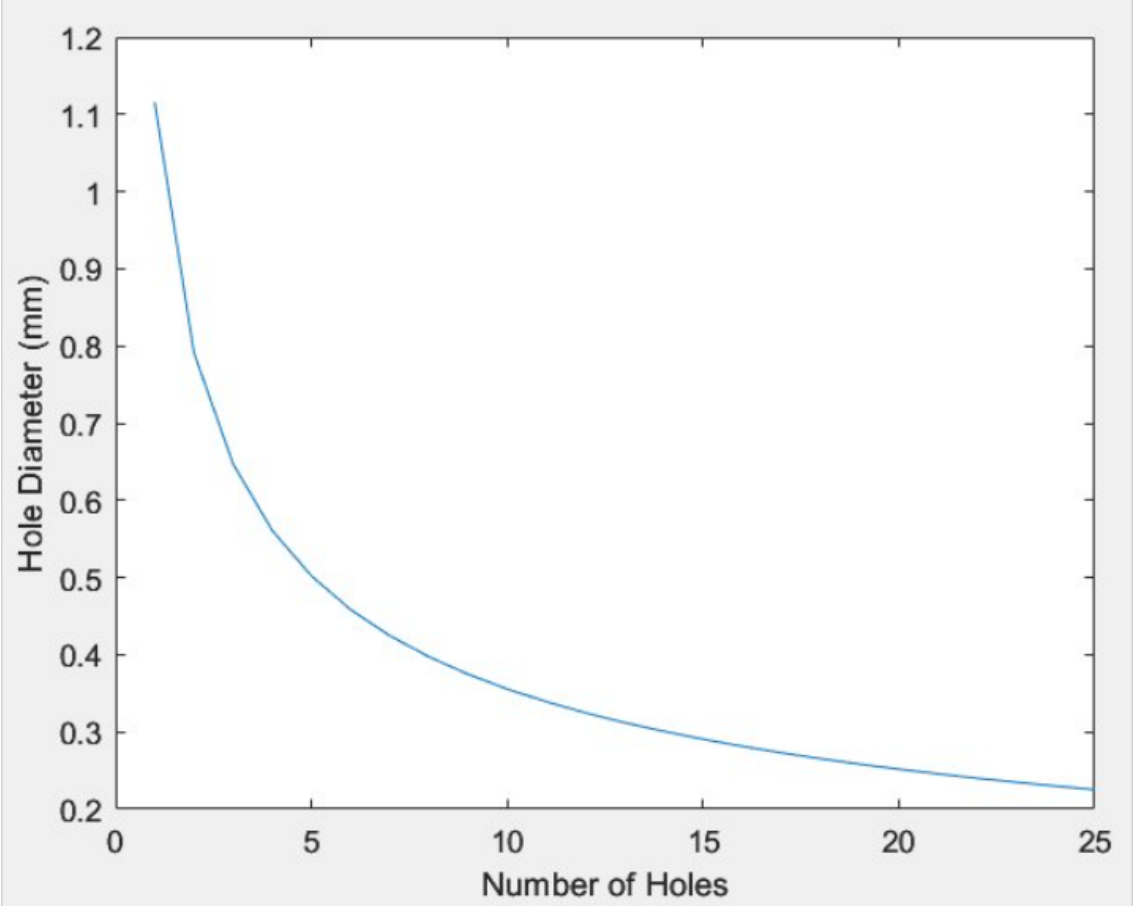

Figure 12: Plot of number of injector orifices versus orifice size for the showerhead injector.

6.4 Components

The components that were purchased to meet the subsystem design requirements are depicted below in Fig. 14.

7 Pyrotechnics Subsystem

7.1 Subsystem Overview

The pyrotechnics subsystem is responsible for initiating combustion within the motor by igniting the fuel grain using a reliable and repeatable ignition source. The ignition must provide enough energy to initiate pyrolysis of the fuel grain, producing gaseous products that can react with the injected oxidizer. This reaction helps decompose the nitrous oxide into nitrogen and oxygen, making it easier to sustain combustion. Ignition must also be precisely timed with the onset of

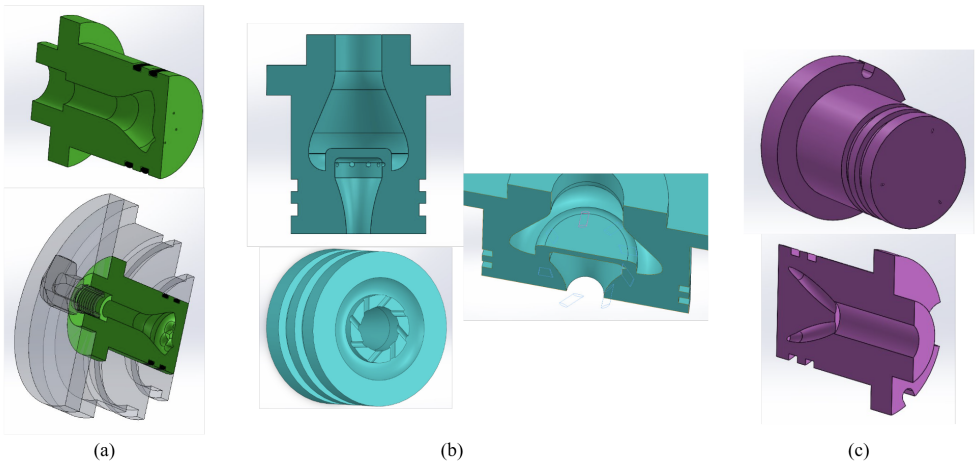

Figure 13: (a) Showerhead, (b) uniaxial swirl, (c) impinging jet injectors.

oxidizer flow to enable sustained combustion and stable thrust generation.

7.2 Subsystem Requirements

This subsystem was designed to meet a series of critical performance and safety requirements that ensure reliable ignition and sustained combustion. The fuel grain must have a single port. To ensure adequate performance, the grain must provide a minimum five-second burn duration with a safety factor of at least 1.2. Additionally, the port area is constrained to fall between 0.28 and 1.70 square inches, a range selected to maintain appropriate regression rates and prevent over-pressurization. Some of the grain geometries are further required to promote a consistent O/F ratio throughout the burn, a condition validated through experimental testing. The system must ensure that the igniter can pyrolyze a sufficient volume of ABS to initiate and sustain combustion. Both the fuel grain and igniter must be easily replaceable to support rapid testing and iteration, a design consideration validated in practice through subsystem assembly and test procedures.

The pyrotechnics subsystem is composed of two primary components: the fuel grain and the igniter. In ATLAS, the fuel grain is 3D printed from ABS plastic and configured in the two geometries previously mentioned ABS has been widely used in hybrid rocket applications due to its moderate regression rate, favorable safety characteristics, and ease of fabrication via additive manufacturing. For ignition, the system uses a Pyrodex pellet ignited by a remotely actuated E-match. This method was selected for its simplicity, reliability, and proven ability to reach the

Figure 14: Assorted oxidizer plumbing components, including analog pressure gauge and servo-actuated ball valves, after cleaning.

ignition temperature required to pyrolyze ABS and initiate sustained combustion. The original configuration of the ignition system within the combustion chamber is shown in Fig. 15.

7.3 Fuel Grain

The fuel grain is 3D printed out of ABS filament, which allowed the easy production of complex geometries for testing. Prior research highlights the critical role of grain geometry in optimizing the O/F ratio and overall motor performance, making it a central consideration in our design process. Several geometries were considered, including gear, cross, flower, and star shapes, each

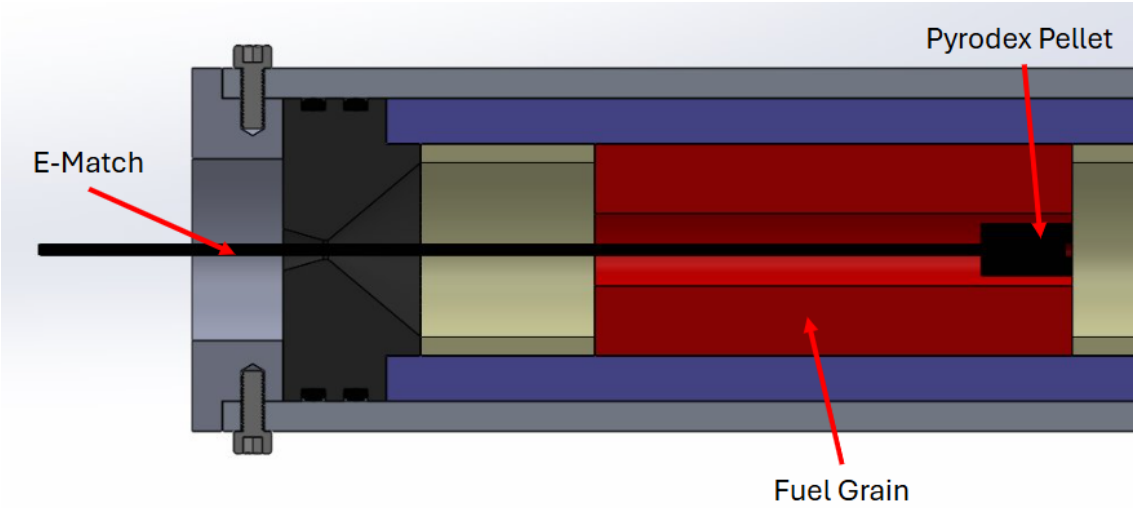

Figure 15: Original pyrodex/e-match ignition system with fuel grain.

with distinct hydraulic diameters and regression characteristics, although only two (circle and cross, see Fig. 17) were planned to be used during hot-fire testing and analyzed. Circular geometry is the most simple design, where, as the fuel burns, the perimeter of the circle grows, changing the O/F ratio. The other geometries were designed to promote stable regression while avoiding over-pressurization through geometry that maintains a constant perimeter-to-area ratio. The star design is representative of these improved characteristics.

Non-circular ports were treated using the equivalent hydraulic diameter, ensuring accurate modeling of oxidizer flow and fuel regression, and allowing for comparisons between designs of differing geometry. Hydraulic diameter was calculated using:

$$D_h = \frac{4A}{p}$$

where A is port area and p is port perimeter. The hydraulic diameter was used in the Marxman regression equation, given by

$$\dot{r} = aG_{ox}^{n}$$

where $\dot{r}$ is the regression rate, G_{ox} is the mass flux of oxidizer through the fuel grain port, and a and n are empirically derived constants specific to the specific engine and propellant characteristics. The Marxman equation was iteratively solved in MATLAB for each fuel grain geometry and used

to size the ports of each fuel grain. Regression plots for radius and grain mass, such as those seen in Fig. 16, were generated for each fuel grain.

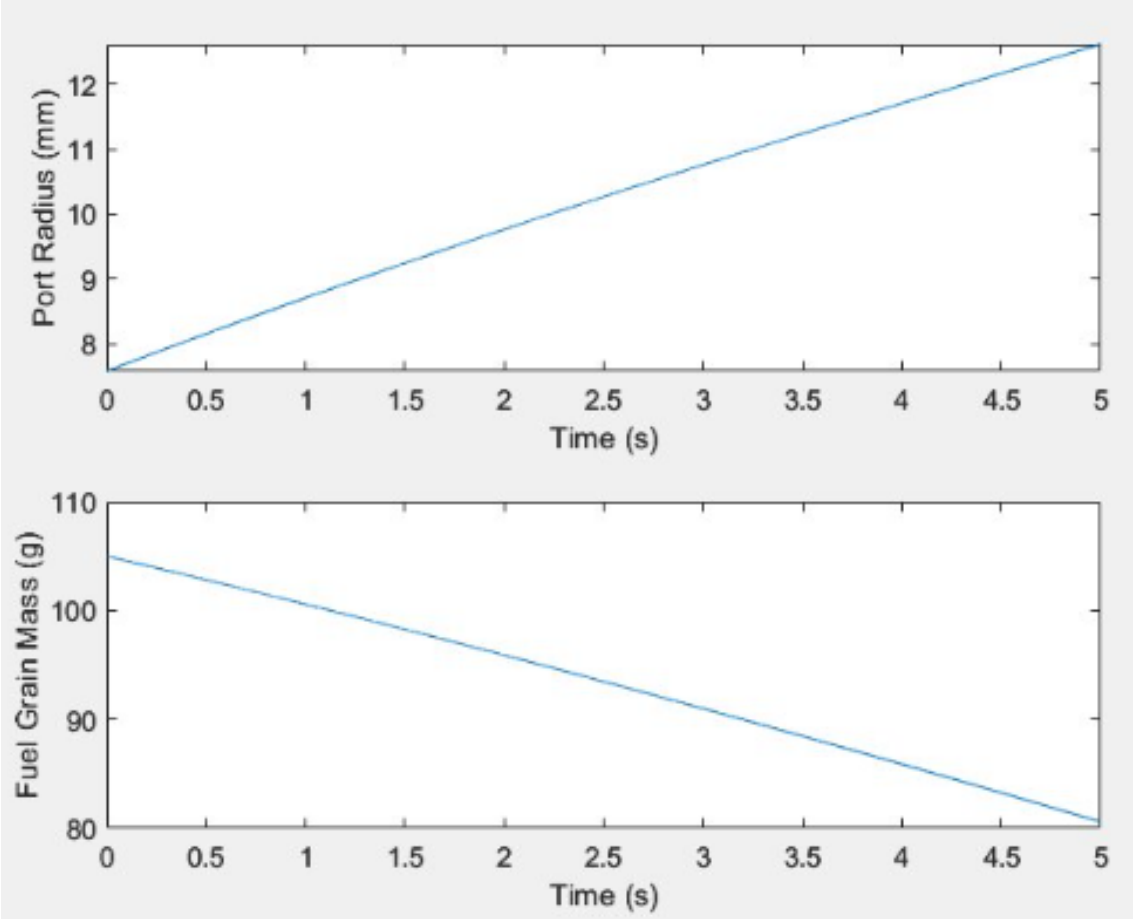

Figure 16: Regression of port radius and fuel grain mass over time for a circular port geometry.

Grain mass ranged from 0.1–0.15 kg, and all designs maintained a minimum wall thickness of 3.525 mm, ensuring the fuel grains did not burn up entirely during the burn. It should be noted that the unburned fuel grain serves as a thermal liner, protecting the other engine components from the high-temperature exhaust gases involved during combustion.

7.4 Ignition Systems

The selected ignition system consists of a Pyrodex pellet ignited remotely using a commercial E-match drawing 24 W of power. Among evaluated ignition methods (pyrotechnic, augmented spark, and torch), the Pyrodex setup achieved the highest composite qualitative score for reliability, cost, and simplicity. Pyrotechnic ignition is frequently used to ignite combustion in rocket engines of

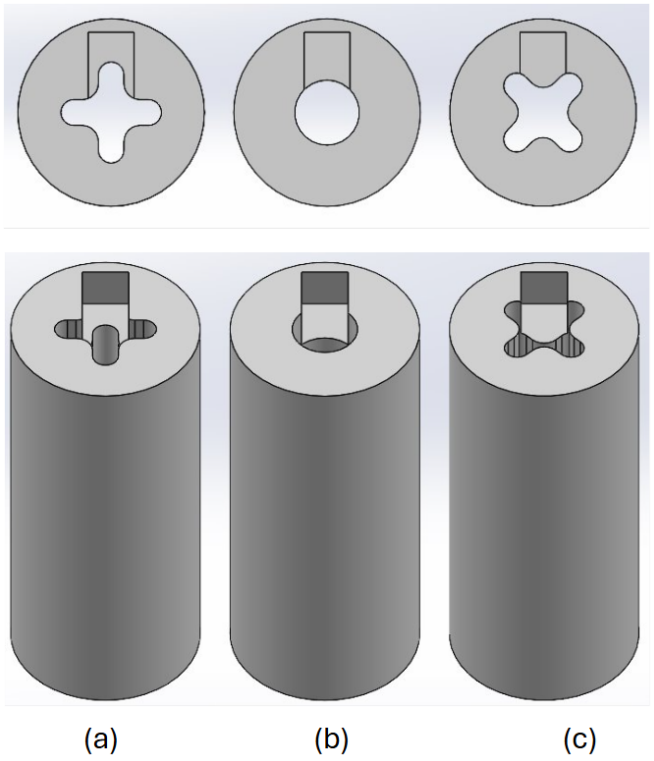

Figure 17: Fuel grains with (a) Plus-Sign 1, (b) Circle, (c) Plus Sign 2 port geometries.

I-class or even much larger, making it an appealing choice for ATLAS. To validate the ability of Pyrodex to pyrolyze a sufficient quantity of ABS, small cross sections of the fuel grain were produced, loaded with pellets, and tested for significant ABS pyrolysis.

The method first selected to fasten the pellet within the combustion chamber was a simple adhesive to hold the pellet in place long enough to pyrolyze the ABS and begin combustion. However, initial testing showed that the high-pressure nitrous oxide flow was blowing the pellets out of place. To solve this problem, fuel grains were redesigned with a notch at the end nearest to the injector to hold the igniter in place while it ignites, as seen in Fig. 18. Small fuel grain samples were printed to test the modified designs and which one could most effectively pyrolyze the ABS. The samples for the ignition system tests are shown in Fig. 19. The highest performance was observed from a design that combined the use of Pyrodex pellet mounted within a cutout in a cross-shaped (plus sign) port geometry. The Pyrodex pellet produced a short hot blast to pyrolyze the ABS and the mass cutout allowed for a flameholding zone, which sustained the burn to ensure a high enough temperature to decompose the N2O into N2 and O2.

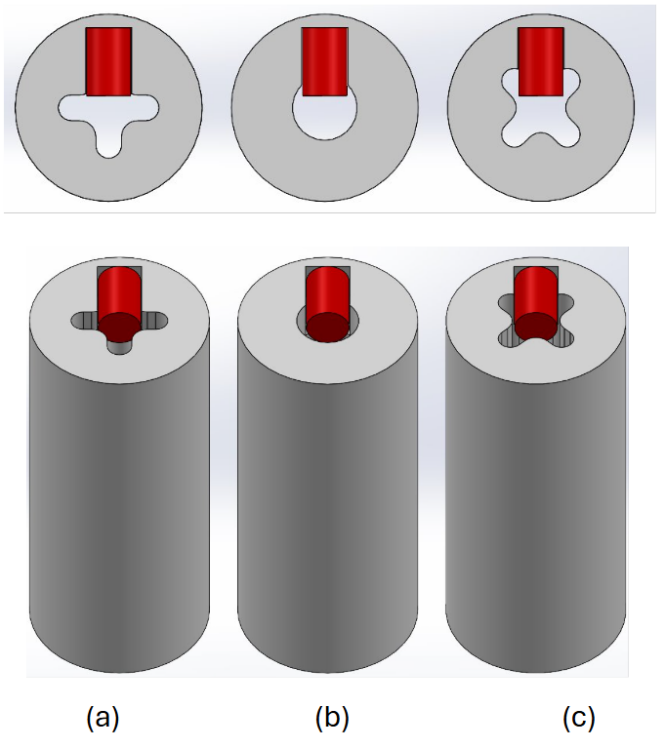

Figure 18: Fuel grains with ignition pellet cutout with (a) Plus-Sign 1, (b) Circle, (c) Plus Sign 2 port geometries.

7.5 Integration and Assembly

The grain and igniter assembly are designed for ease of insertion and replacement in the combustion chamber. The modular design enables fast turnaround during testing while maintaining safe handling procedures for energetic materials.

7.6 Testing

Multiple configurations of the pyrotechnics subsystem were tested to determine which was best for usage. To test, subsections of fuel grains were printed and tested with various igniter setups. After some initial testing, it was determined that a cutout should be added to the design in order to limit the possibility of a pellet becoming dislodged and clogging the nozzle and in order to pyrolyze the ABS in the most efficient matter based on the directionality of the ignition. Test samples were weighed before and after ignition and videoed in order to determine the ideal setup based on the change in mass and on visual cues. Seen below in Fig. 20 is a circular fuel grain port with a cutout

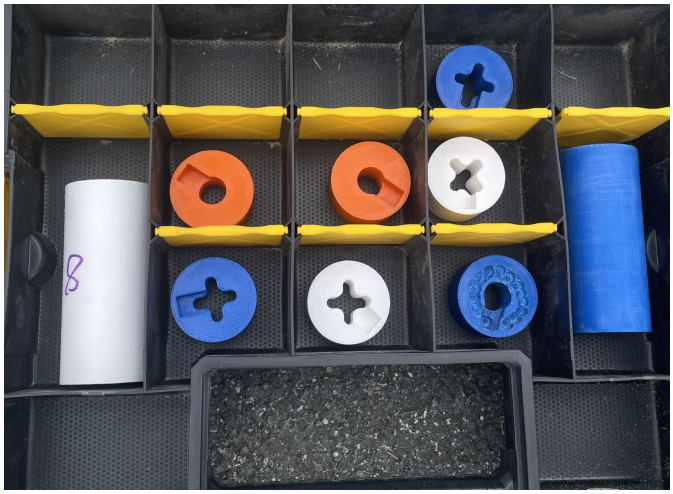

Figure 19: 3D-printed ABS plastic fuel grain samples used for ignition system testing.

for a Pyrodex pellet.

8 Ground Testing Subsystem

8.1 Subsystem Overview

The ground testing subsystem performed several critical functions. Primarily, it served to ensure safe execution of static hot-fire tests. It was comprised of a test stand, blast shields, data acquisition components, and control system.

8.2 Test Stand

The test stand, shown in Fig. 21, was designed to constrain all other subsystems while allowing thrust data to be gathered. This was accomplished by creating the 80/20 aluminum frame and attaching it to cinder blocks using masonry screws. The frame provided a location to mount the oxidizer tank with a 1/8-inch thick steel shield between it and the combustion chamber. The frame allowed space for the plumbing system to be mounted to the furthest back 80/20 strut. A set of linear rails were bolted to the stand. Steel strut channel was mounted to the bearing blocks that interface with the linear rails. The strut channel enabled high-strength strut clamps to secure the combustion chamber. When assembled, the system allowed roughly one inch of low-friction, linear

Figure 20: Circular fuel grain With Pyrodex cutout during ignition system testing. Note presence of blast shield with polycarbonate viewing panel.

movement along the thrust direction of the engine. This single degree of freedom enabled the data acquisition system to gather thrust information. The final design is shown in Fig. 21.

The structure was analyzed considering the expected 60-Newton thrust. SOLIDWORKS finite element analysis (FEA) was used on a model of the stand but with simplified joints to determine the joints under the greatest stress. This analysis, shown in Fig. 22, showed that the joints to consider were those at the top and bottom of the central column that would hold the load cell. Hand calculations were used and determined that the bolted connections had a safety factor greater than 50. The second most stressed joint was where the horizontal member at the bottom of the column met the side rails. The standard 80/20 bracket hardware would rely on friction to secure that member instead of actual bolt strength. To ensure a high-strength joint, bolts were installed

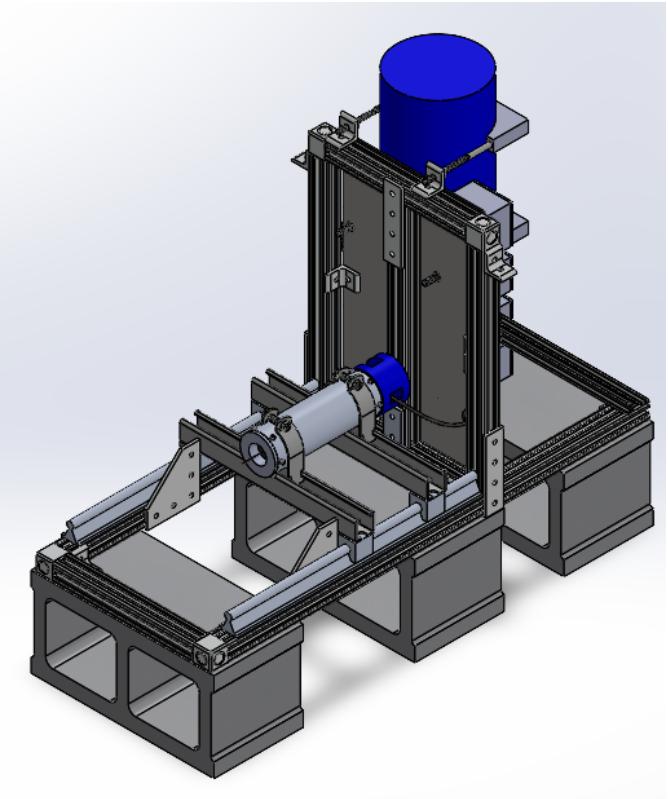

Figure 21: Test stand assembly with oxidizer system, combustion chamber assembly, and control boxes.

through the long side rails and directly into the horizontal member, and additional masonry screws were used to attach it to the cinder block. The stand was also analyzed for stability by completing a sum of moments about the point marked in Fig. 23. With the stand connected to three cinder blocks using masonry screws, the analysis showed a safety factor greater than ten for tipping.

8.3 Blast Shields

In addition to the steel sheet on board the test stand, large mobile blast shields were constructed to ensure personnel safety against catastrophic motor failures. A sixteen-gauge steel sheet was mounted to a frame. The frames consisted of standard wood pallets supported by 2x4 assemblies. Cinder blocks were placed on the horizontal cross members of the 2x4 assemblies to provide additional stability. They were constructed using gussets, connector screws, and heavy gauge GRK screws. To provide a protected area for a thermal camera, part of one of the blast shields was made of 1/4 inch polycarbonate sheet instead of steel. Polycarbonate is known for its high resistance

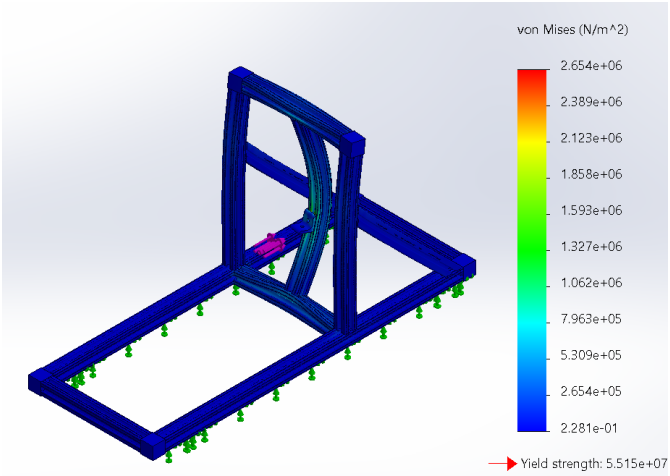

Figure 22: Simplified test stand static structural FEA in SOLIDWORKS.

to ballistic and explosive damage, being 250 times more impact-resistant than safety glass [Rossi, A, 2022]. The camera was mounted behind the polycarbonate to give it a protected view of the exhaust stream from the motor. These 36" by 48" blast shields are shown in Fig. 24.

8.4 Data Acquisition

The data-acquisition (DAQ) subsystem was implemented to obtain time-synchronized measurements of pressure, temperature, thrust, and high speed video during static fire trials. The hardware consisted of an ESP-32S development board for sensor interfacing, a Raspberry Pi 4 B (8 GB) as the primary DAQ computer, and the following sensors: two gauge pressure transducers, two K-type thermocouples, and a 10 kg load cell. The pressure transducers were mounted immediately upstream and downstream of the injector to capture the differential pressure across the injector throat, enabling the validation of the injector performance. One thermocouple measured ambient conditions, while the second was installed within the combustion chamber to confirm sustained combustion. The load cell was aligned coaxially with the thrust axis to record instantaneous thrust force.

The sensor signals were conditioned and digitized by the ESP-32S, which performed the following functions in real time: 1. Reading of the analog voltage output of each pressure transducer and each thermocouple. 2. Retrival of digital load cell readings via the I2C interface. 3. Serialization of all five raw measurements into a single UART data frame transmitted to the Raspberry Pi over

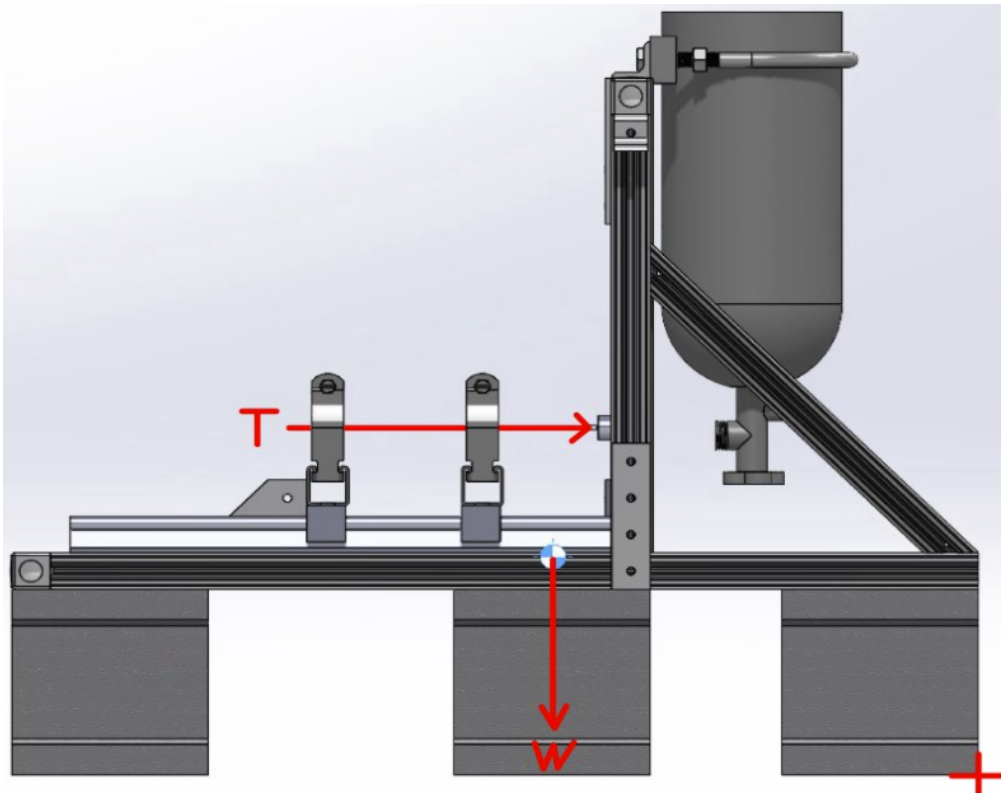

Figure 23: Static analysis of stand stability, demonstrating that the stand will not tip over under operational loads.

a serial link.

Upon receipt, an ROS-enabled serial node (serial_node) on the Raspberry Pi demultiplexed the data stream into individual raw-voltage topics. A subsequent calibration node (conversion_node) subscribed to each raw topic, applied sensor-specific conversions, and republished the results (pt_value, tc_value, loadcell_value). These calibrated data streams were recorded and visualized in real time via a PlotJuggler listener node (Fig. 25).

Concurrently, a second Raspberry Pi interfaced with a FLIR camera via a vendor-supplied FLIR Spinnaker nodelet manager and an image-processing debayer nodelet. These video frames were published and then compressed for live monitoring and recording.

8.5 Control System

The control system distributed responsibilities across three ROS-enabled computers on a dedicated Ethernet LAN. Two Raspberry Pi 4 B "edge controllers" handled hardware-level interfacing, and

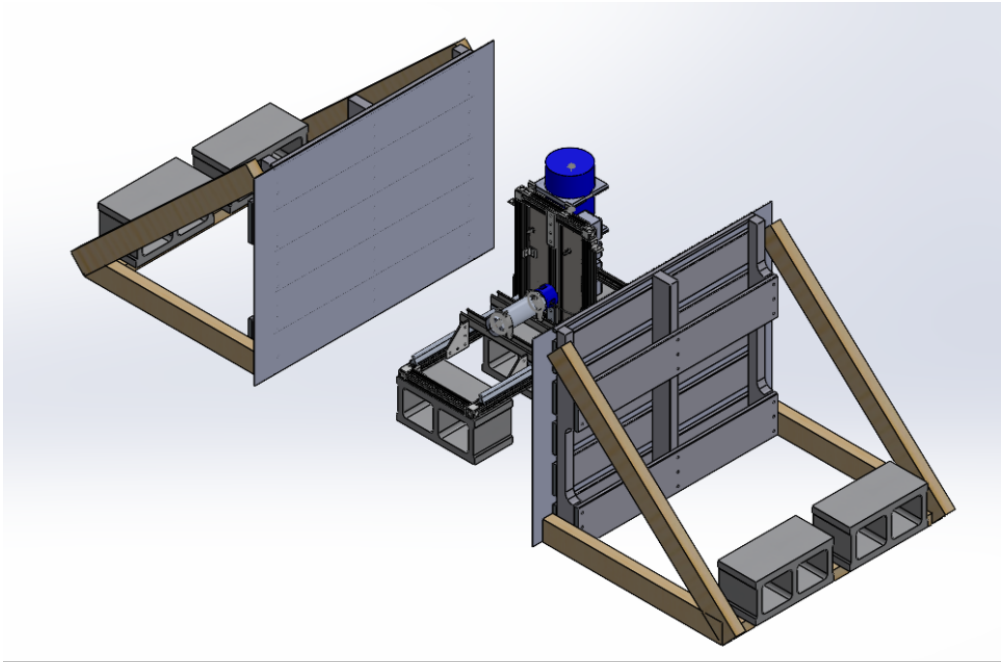

Figure 24: Test stand assembly with blast shields.

a central workstation provided visualization, user controls, and remote access.

Edge Controller A combined data acquisition, valve actuation, and ignition timing. It unpacked raw sensor readings from the ESP-32S and republished calibrated pressure, temperature, and thrust topics; generated PWM signals to two 35 kg·cm servos on the nitrous-oxide ball valves via the `/servo_angle` topic; and offered a ROS service to trigger ignition relays with millisecond precision. Co-locating these functions ensures deterministic execution of all safety interlocks and time-critical commands.

Edge Controller B ran the FLIR Spinnaker SDK and a debayer nodelet, publishing live video at up to 160 fps. Offloading imaging here prevents high-bandwidth video from impacting edge-control timing.

The main workstation ran a GUI node presenting live telemetry plots (via PlotJuggler), an embedded FLIR video display, and interactive controls for servos and ignition (Fig. 26). It also provided SSH access to both Pis for diagnostics and emergency shutdown. This layered design keeps safety-critical control at the edge independent of host-level visualization, so edge controllers continue operating even if the GUI or network falters.

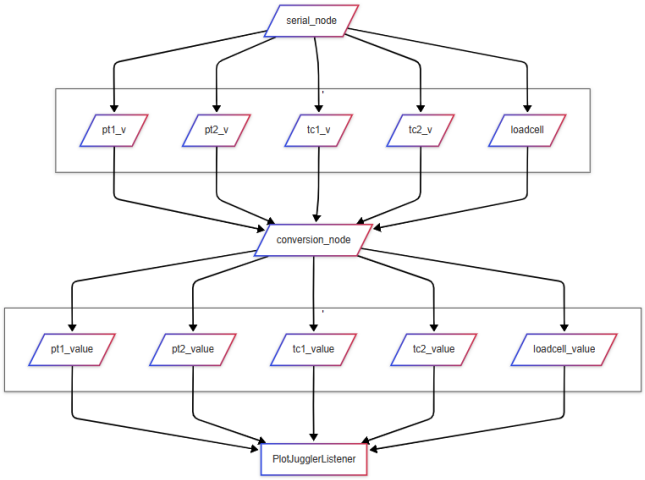

Figure 25: Sensor conversion flow chart.

9 Test Campaigns and Design Validation

9.1 Hydrostatic Test

Hydrostatic tests on the combustion chamber were performed to validate the structural integrity of the design and the functionality of the seals. The test procedure began with assembling the combustion chamber with a few notable modifications. Instead of the graphite nozzle, a 3D printed nozzle with no through hole was installed. A modified injector (Fig. 27) was used to connect a pressure washer hose where the oxidizer line goes in the hot fire configuration. Once the engine was assembled in this orientation, a pressure washer supplied water to the combustion chamber until chamber pressure reached 1000 psi (more than double the pressure expected during a hot fire). The pressure in the chamber was then monitored for 30 minutes to ensure structural integrity and no leaks within the system.

A few notable adjustments were made following hydrostatic testing. Chiefly, the assembly process was iterated on. All components were manufactured to very tight tolerances which ensured no leaking, but also made assembly difficult. Clamps were utilized to compress the nozzle and nozzle bulkhead into the combustion chamber. While initially promising, under further inspection, this process damaged the O - rings on the nozzle. To minimize O - ring damage, additional components were manufactured to cover the radial holes on the combustion chamber and to gently compress the O rings to allow for an easier fit. This modification minimized damage to the O -

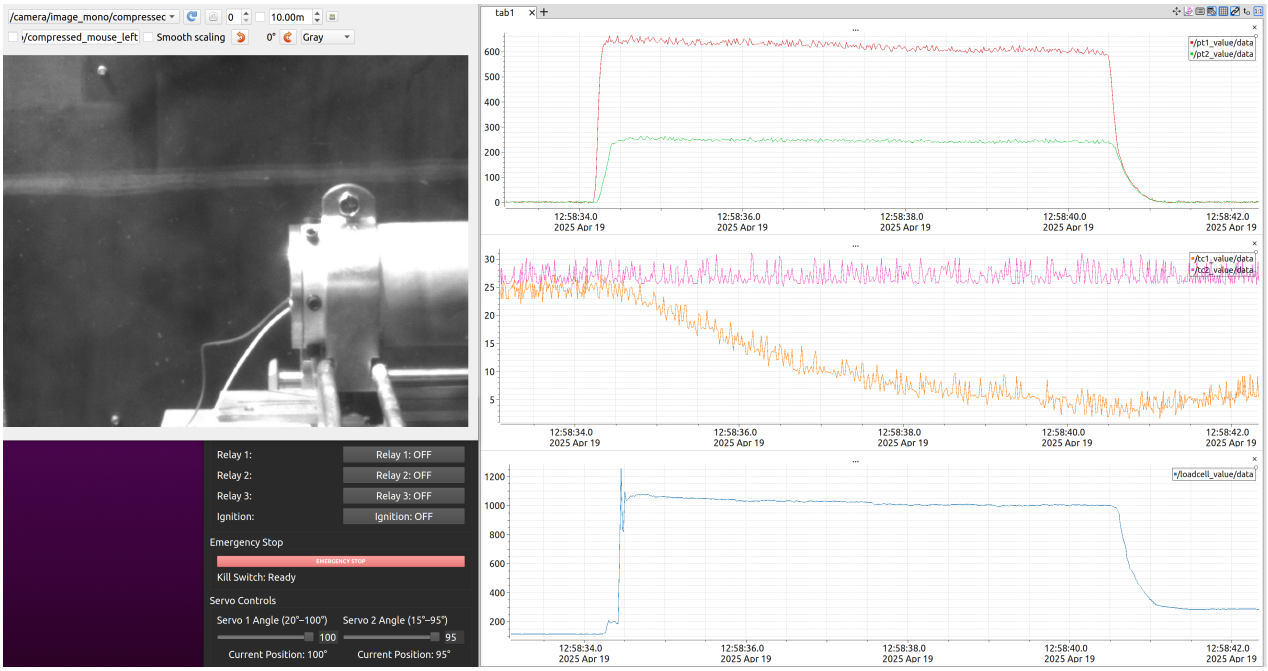

Figure 26: Example image from main workstation user interface and data streams.

rings and optimized the assembly process. The hydrostatic test setup is depicted in Fig. 27.

9.2 Cold Flow Test

Once the engine system and test stand were completed, the entire design was validated through a cold flow test campaign. This involves testing every component in a "dry-run" of the hot fire. Everything is operated as planned during a hot fire test, minus the ignition system. Once the system was fully assembled, all team members left the 100-ft safety radius except for the test lead and safety officer. The solenoid valve was opened and closed to ensure functionality. Once confirmed, the test lead opened the needle valve and the oxidizer tank and everyone evacuated the test zone. The solenoid valve was opened and oxidizer began to flow, as depicted in Fig. 28. After 5 seconds the solenoid was closed, however an issue with the valve prevented the system from fully closing which resulted in a slow leak of oxidizer. Data was collected by the DAQ system and analyzed for future testing. The test lead proceeded to the stand to shut off the oxidizer tank from the bottle.

When analyzing these data, it was apparent pressure drop (Fig. 29) between the tank and the combustion chamber was far too high. It was determined large losses were occurring at the needle

(a) Hydrostatic test setup.

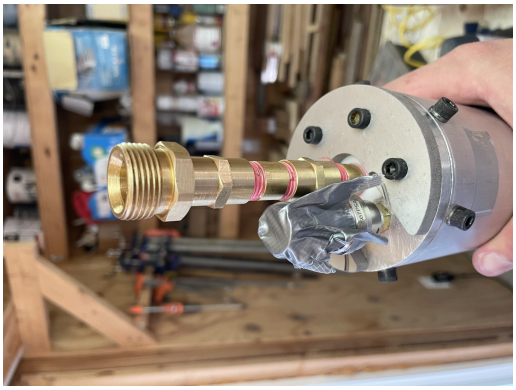

(b) Hydrostatic injector bulkhead plumbing.

Figure 27: Sample images of hardware modified for hydrostatic test.

Figure 28: Nitrous oxide exhaust stream during cold flow test.

valve and at the solenoid valve. After disassembling the oxidizer system it was determined that debris from the Teflon tape utilized to attach the fittings had clogged the solenoid. To prevent such an issue in hot fire all of the plumbing was cleaned using chemicals and a ultrasonic cleaner and from this point on all plumbing was only handled by people wearing gloves. Additionally, Teflon tape was replaced with Teflon paste. To solve the issue of the solenoid not fully closing and the large pressure drop, the needle valve and solenoid were replaced by two ball valves each remotely controlled by servos. This required multiple adjustments to the ignition sequence, all of which were later confirmed visually using a multimeter to ensure correct ignition timing in relation to servo actuation. Furthermore, the new configuration underwent additional cold flow tests to

confirm pressure drops and proper opening and closing of the ball valves. Thrust data are also depicted in Fig. 30.

Figure 29: Pressure (psi) versus time (ms) data for cold flow test with needle valve at 50% open position.

9.3 Static Hot Fire Test

After the cold flow tests were completed and the valve states and plumbing adjusted according to the test results, the engine was then hot-fired. The first three attempts were used to calibrate the ignition timing with the oxidizer release. If the ignition system goes off before the oxidizer enters the chamber in meaningful amounts, there is no combustion and the hot-fire becomes a cold flow test. If the ignition system is activated too late, long after the oxidizer has entered the chamber, this can result in the ignitor flame being snuffed or a hard start event, where the chamber

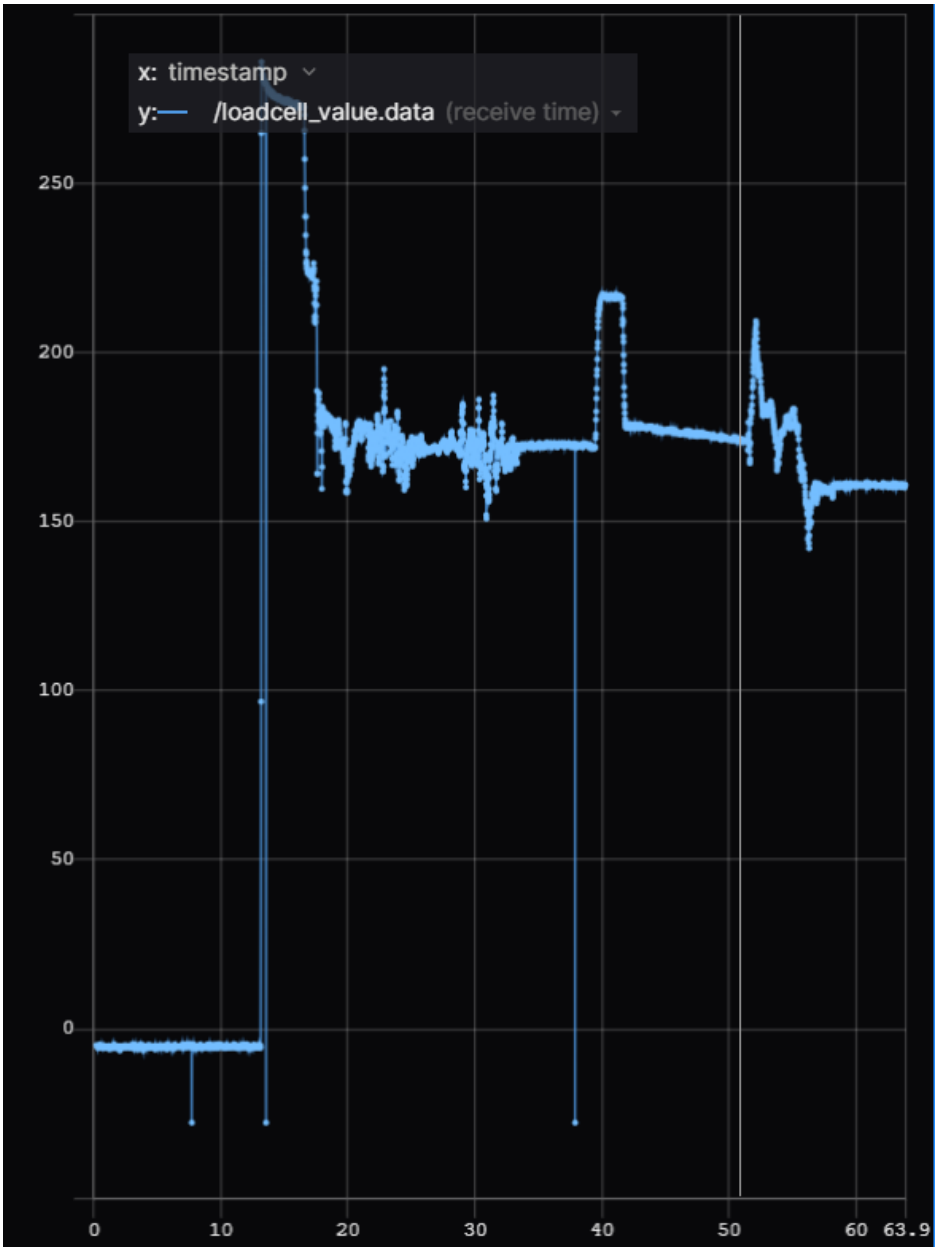

Figure 30: Thrust (N) versus time (ms) data for cold flow test with needle valve at 50% open position.

experiences a pressure spike far above operational loads and runs the risk of structural failure.

The fourth hot-fire attempt resulted in failure of the engine bulkheads via tearout stress and bolt shear, as shown in Fig. 31. Forensic test footage demonstrated that the high flow rate of the oxidizer, elevated due to the large pressure differential between the oxidizer tank and the ambient air within the chamber, dislodged the ignition pellet. This caused the pellet to travel down the fuel grain and lodge within the nozzle, after which it was ignited. The rapid pressure increase within the chamber blew both bulkheads off the chamber, effectively destroying the entire engine and damaging portions of the test stand. The progression of the ignition cables down the engine is depicted in Fig. 32.

Figure 31: Failure of nozzle bulkhead during hot fire attempt four.

The team then ran another round of ignition tests with a redesigned fuel grain and ignition system designed to prevent the pellet from becoming dislodged. This design incorporated a shelf within the fuel grain to which the ignition system could be glued. The shelf also incorporated a flame holding cavity in which the flame from the ignition system could easily pyrolyze fuel while avoiding the high mass flux stream of oxidizer. These ignition tests were more successful than the original ignition system tests, indicating that the system increased the likelihood of combustion while greatly reducing the risk of clogging the nozzle. Additionally, the ignition cables were redesigned to have a smaller footprint and dissolve more easily when exposed to operational

(a) (b)

(c) (d)

Figure 32: Ignition cables traveling down the engine, indicating failure due to nozzle clogging.

temperatures, further reducing the risk of a clogged nozzle.

The team rebuilt the engine (see Fig. 33b), refurbished the stand, and designed these new ignition systems within five days of the engine failure in preparation for the next round of testing. The plumbing system remained unchanged, as all components were hydrostatic tested for integrity and found to be ready for operation. This meant that the injector introduced such a high pressure drop to upstream flow that the check valve and other oxidizer supply hardware were undamaged, meaning that the system designed to prevent backpressurization functioned properly. The fuel grains and ignition cables were redesigned to prevent clogging of the nozzle. The ignition cables were slimmed down, switching from standard insulated wires to copper wires used in motors. In addition, the ignition system and fuel grain were redesigned to prevent nozzle clogging by securely mounting the ignition system and increasing the burn time, as mentioned in section 7. The ignition systems were also hot-glued to the fuel grain to prevent them from becoming dislodged. The test stand was strengthened by solidifying the support on the blast shield, ensuring it was firmly attached to the cinder blocks. The remainder of the design was left unchanged for consistency, as the cause of failure resided in the fixation of the fuel grain.

Unfortunately, further testing was canceled due to evolving requirements in the test approval

(a) ATLAS I combustion chamber before testing.

(b) ATLAS II combustion chamber before testing.

Figure 33: Comparison of ATLAS I and ATLAS II combustion chambers. ATLAS I was destroyed during testing.

process dictated by UVA safety and risk management officials (as of the writing of this document). Future testing must be conducted by successive cohorts of capstone student teams. The ignition timing must first be honed in, then the throttle valve calibrated for each injector being used. Once tests are consistent and yield predictable results, the fuel grains and injectors can be swapped out between tests.

10 Risks and Mitigation

A summary of expected risks and the team's plan to mitigate these risks is outlined in Appendix C. While there were many risks that could occur during the testing, Team Atlas has made plans to prevent these risks from occurring and also mitigate their effects. Tjhe ATLAS safety officer is depicted in Fig. 34. The procedures and measures outlined in the appendix are able to be easily adapted for future rocketry projects here at the University of Virginia and are flexible enough to fit many different rocket types.

Figure 34: ATLAS test stand setup with safety officer performing safety checks.

11 Conclusions

Aerospace Engineering Capstone Team 3 developed ATLAS, an H-class hybrid rocket engine and supporting ground testing system in partial fulfillment of the requirements for the 2024-2025 MAE 4790/4800 capstone courses. The engine was designed to fire for five seconds at a time, producing 14.4 pounds of thrust with a chamber pressure of 500 psi and temperature of 3300 K. The team subjected the analytical design to preliminary and critical design reviews, then analyzed all components using state-of-the-art analysis software. The engine was then manufactured in the early months of the Spring 2025 academic term. The team passed the engine through hydrostatic and cold flow test campaigns, which it passed. The engine was destroyed during the hot fire test campaign due to a clogged nozzle and rebuilt within a week. The current design is awaiting approval for testing.

The ATLAS hybrid rocket engine serves as a testbed for innovative fuel grain and injection system designs that leverage the cutting edge of additive manufacturing technology. In addition,

ATLAS is a catalyst in that it is the first student-built propulsion system at UVA and serves as a prototype for UVA's competition-scale hybrid engine, PROMETHEUS.

Future work remains to be done on the engine. The ignition timing must be found carefully for each ignition system used. All future hot fires should implement the revised fuel grain/ignition system design which prevents nozzle clogging.

Once hot fires can be consistently achieved, a test matrix should be designed for each combination of fuel grain geometry, injector geometry, and throttle valve position. While system hardware allows, each combination should be tested and pressure, thrust, temperature, and video feed data logged. Regression rate coefficients and mass flow rates should be calculated for each combination. If more testing can be conducted, each combination should be repeated 1-2 more times to examine consistency. These results are of great interest to the hybrid rocket engine community, and the continuation of this study would make for an excellent independent research project.

Appendix A: Teams and Roles

Figure 35: Fall 2024 team breakdown structure.

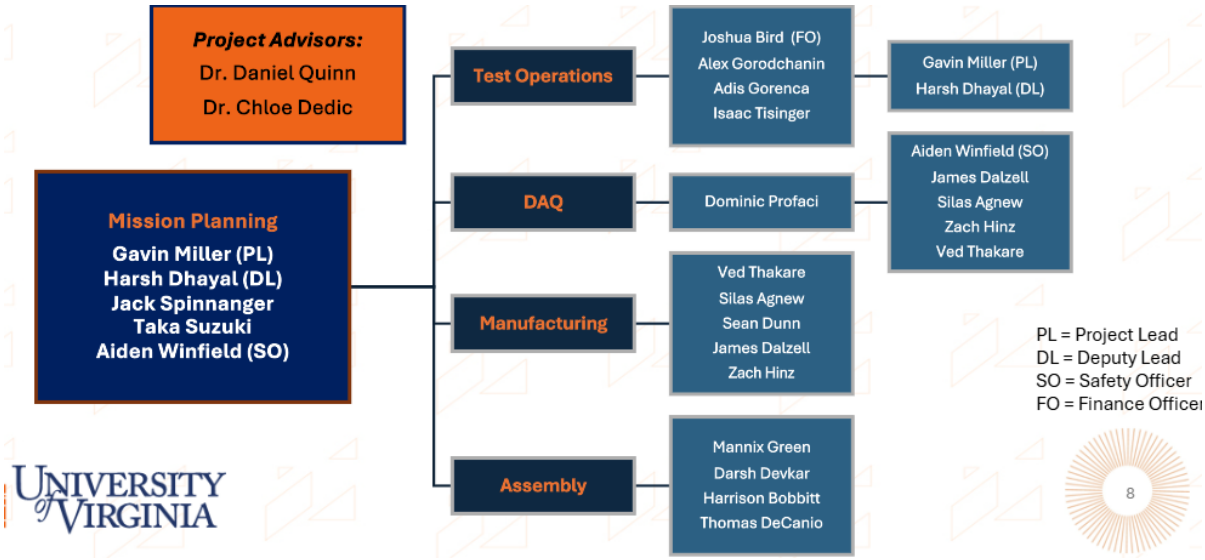

Figure 36: Spring 2025 team breakdown structure.

Figure 37: A portion of the Project ATLAS capstone team.

Appendix B: Financial Budget

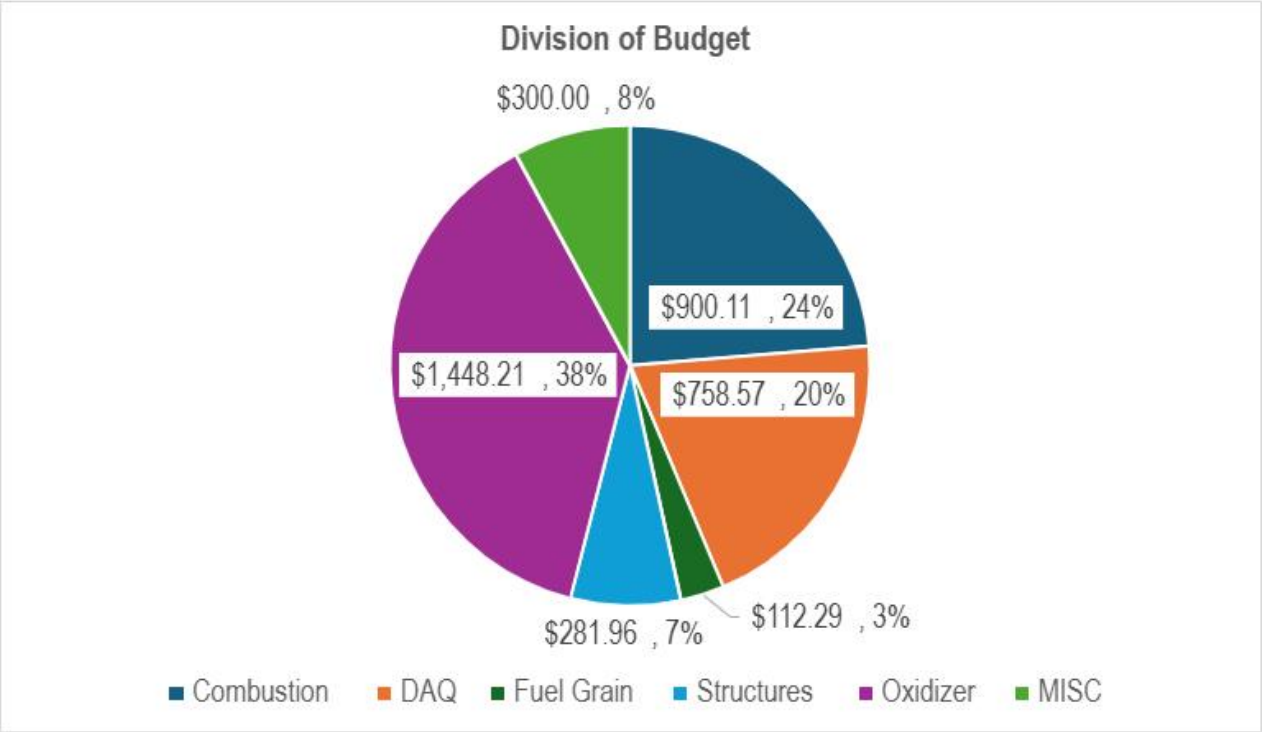

Figure 38: Pie chart breakdown of total system cost by major subsystem teams. Expenditures shown are from a total budget of $4550.

Appendix C: Risks and Mitigation

Risk ID	Risk Name
R1	Manufacturing Training
R2	Valves Arrive Late
R3	Burst From Over Pressurization
R4	Testing Site
R5	Pay For Rapid Shipping
R6	Bad Data
R7	Manufacture Time Goes Past March
R8	Engine Not Well Secured
R9	Injector Melts

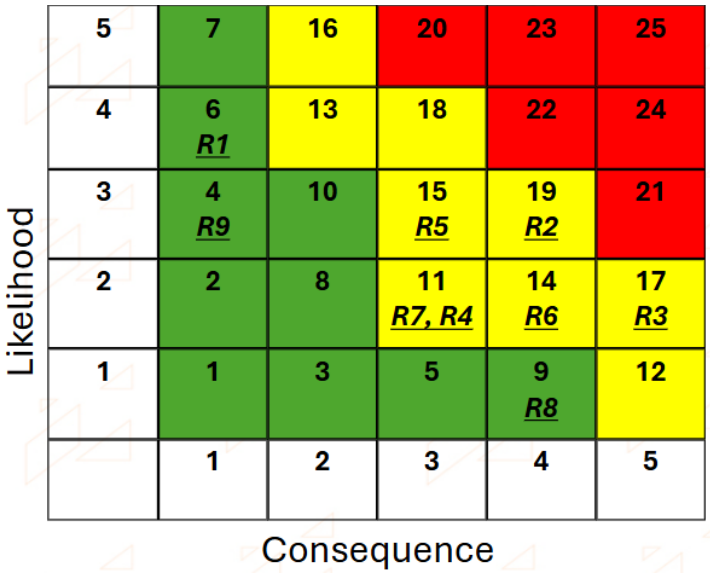

Figure 39: Sample risk matrix for Project ATLAS in accordance with NASA standards.

Risk	**Countermeasure**
Thermal runaway/rupture of main engine; associated danger to surroundings	Two 3' x 4' metal blast shields to protect surroundings, along with one smaller shield to protect sensitive components.
Over-pressurization of Engine	High-quality sensors able to detect over-pressurization and automatically shut off oxidizer flow (kill engine). Relief valve directly upstream of injector set at 655 psi.
Over-pressurization of Oxidizer Tank	Relief valve mounted to tank set at 700 psi. Testing will not be conducted unless ambient temperature is less than 95°F.
Ignition of engine during setup	Ignitor will be mounted as the last step before clearing area; in the meantime, oxidizer will remain in tank.

Risk	**Countermeasure**
Ignition of engine with students nearby	Team and bystanders will remain a minimum of 100 feet away while the range is hot. Ignition sequence will be remotely actuated. Ignition control setup will be near buildings capable of providing internet.
Human error within ignition timing	Ignition system will be automated to ensure proper timing and sequence. Will be tested thoroughly beforehand without energetic materials. Tests will be monitored by camera. Ignition control setup will be near buildings capable of providing internet.
High-pressure oxidizer lines	Team will remain 100 feet away while plumbing is pressurized. Oxidizer system pressurization will occur as the last step before the test zone is cleared.
Engine not properly secured to stand	Engine will point into structural brace against blast shield. Stand will be bolted to cinderblocks for stability.
Oxidizer tank catching fire	Blast shield separating oxidizer tank from main engine.
Ground beneath exhaust stream catching fire	Engine shall be set up over a paved surface.
Small fires in vicinity of test stand	Testing will be conducted near a water hookup. Watering cans and fire extinguisher will be kept on hand at all times.
Uncontrolled fire; surroundings catching fire	Testing will only be conducted on days/times deemed acceptable by VDF: risk levels 1, 2, or 3. Test stand will be set up on paved, non-flammable surfaces. Mow adjacent grass as short as possible. Exhaust stream shall be directed away from all foliage and structures. Fire department will be notified and attend test if they determine it appropriate. First test will be attended by fire department.

Risk	**Countermeasure**
Fire risk due to wind	Testing will only be conducted when NWS wind speed predictions are less than 15 mph.
Projectile damage to operators	Eye protection shall be worn by all operators during and after the oxidizer tank is installed, as well as all test attendants within 200 feet of the test site during the test sequence.
Hearing damage to operators	Ear protection shall be worn by all operators and attendants within 200 feet of the test site after installation of the ignitor.
Chemical damage to operators	Nitrile gloves shall be worn when handling any components relating to the oxidizer supply system.
Improper installation of test articles	Test article installation shall be overseen by two designated members of the Test and Integration team. A checklist shall be followed and submitted to the safety officers.
Improper data acquisition and control of system	DAQ and control of system shall be overseen by two designated members of the DAQ and Control team. A checklist shall be followed and submitted to the safety officers.
Improper procedural order	Safety checklists, based on the procedure outlined above, will be given to two designated safety officers to ensure all tasks pertaining to the test sequence are performed and in the proper order.
Interruption of test by unauthorized personnel	Milton Airfield and all associated organizations will be notified of testing window one week in advance. Signage will be placed on major walkways during the testing window. Safety officers will continuously monitor area for unauthorized personnel. Bystanders shall remain 200 feet from test stand at all times.
Distractions to team	Individuals not authorized by the team will be asked to avoid the test stand site, even during setup and takedown.

Risk	**Countermeasure**
Manual ignition of engine, out-of-sequence	Two-stage ignition process shall be required. Safety officer shall possess ignition key until all required checklist items have been completed. Test lead shall then take charge of key and begin the ignition process.
Individual must enter the test zone for some emergency reason	Engine will be immediately disarmed remotely. After 10-minute wait period, ignitor will be removed and test site declared cold by safety officer and test lead. Entry then permissible.
Tipping of test stand or blast shields	Center of gravity designed to be as low as possible on all test articles. Multiple cinderblocks shall be used to weigh down each test item. Staking or partial burial shall be used to anchor articles if test site permits.
Unexpected behavior of control system or engine during fire	Three team members shall monitor live test data at all times. Manual shutdown sequence shall be armed at all times during the test sequence.
Unexpected burning of propellants after engine shutdown	Team shall wait 10 minutes following engine shutdown before approaching test stand. Sensor data shall be continuously monitored to ensure behavior is as expected.
Skin burns from hot test articles	Team shall wait 30 minutes following engine shutdown before handling test articles or engine proper.
Unexpected serious injury during setup or takedown	Potentially dangerous tasks, designated above, shall always be performed by two individuals—"Buddy System".

Risk	**Countermeasure**
Accidental combustion of propellants outside test setup	Oxidizer, fuel grains, and ignition pellets shall all be stored separately and only brought together on the test stand.

Appendix D: Power Budget

The power distribution system was powered via a single standard 120V AC wall outlet combined with outdoor extension cables. The 120V AC was converted into 24V DC power and then stepped down for the remaining relevant electrical and electronic subsystems.

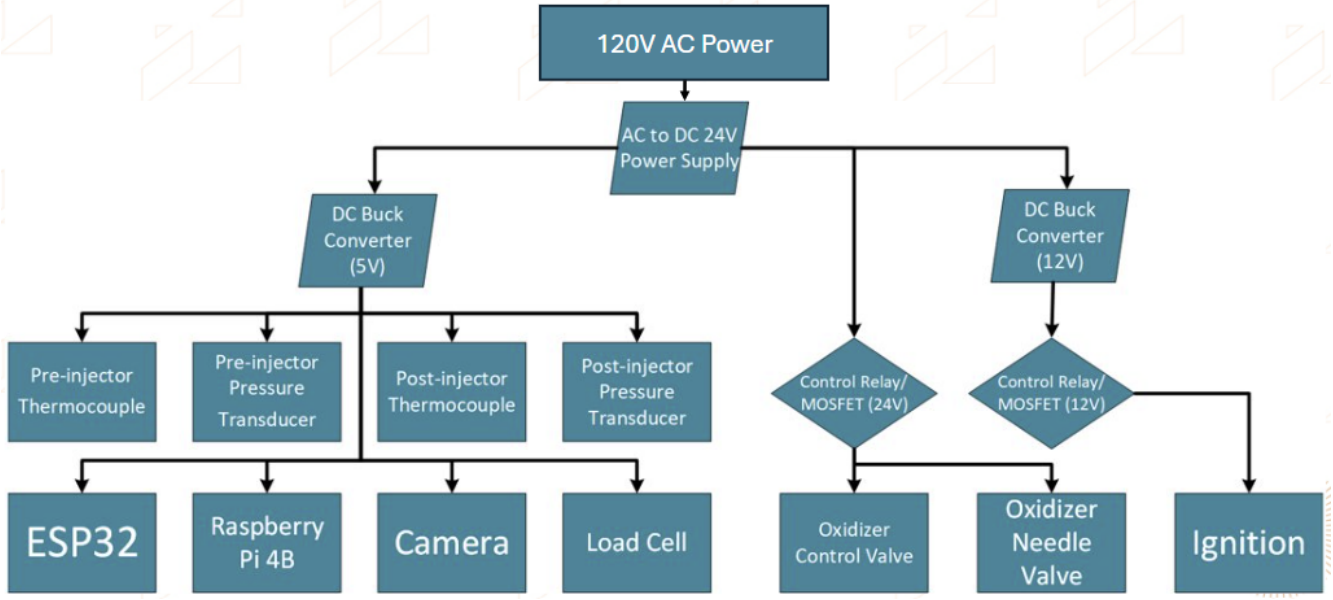

Figure 40: Power distribution flow chart.

5 V Input Devices

Component	Max Current Draw (mA)	Count	Current Sum (mA)
ESP32 Dev Kit	500	1	500
Raspberry Pi 4B 8GB	1540	1	1540
Pressure Transducer	20	2	40
Thermocouple (amplifier)	5	2	10
Load Cell (amplifier)	1.5	1	1.5
Max Total Current for 5 V Supply (A)			2.092

12 V Devices

Component	Max Current Draw (mA)	Count	Current Sum (mA)
Igniter	2000	1	2000
Max Total Current for 12 V Supply (A)			2.000

24 V Devices

Component	Max Current Draw (mA)	Count	Current Sum (mA)
Control Valve	420	2	840
Max Total Current for 24 V Supply (A)			0.840

Total Current Required (A): 4.932

Appendix E: Pressure Drop Calculations

Major loss ΔP across the line

$$\Delta P = f \frac{l}{d} \frac{1}{2} \rho u^2 \tag{11}$$

where

$f = 0.0275$	Friction factor
$l =$	Line length
$d =$	Pipe diameter
$\rho =$	Nitrous density
$u =$	Flow speed

Minor loss Δp across the line

$$\Delta p = K_l \frac{1}{2} \rho u^2 \tag{12}$$

where

$K_l =$	Loss coefficient

References

[Dundas et al., 2018] Dundas, K., Golfogel, A., Grant, C., Grebovic, A., McIrvin, T., Ott, L., Tong, S., Baron, R., Blake, C., Blumhagen, E., Campbell, C., Cassayre, A., Chau, K., Damir, J., Ha, J., Kawaguchi, B., Khairi, A., Kim, E., Ragan, J., Simpson, K., Taverne, J., Walker, M., and Woo, J. (2018). Boundless 2018: Team 09 project technical report to the 2018 spaceport america cup. Technical report, University of Washington.

[Momot, M, 2023] Momot, M (2023). Lecture 22 Thick Walled Cylinders.

[Newlands, 2017] Newlands, R. (2017). *The Science and Design of the Hybrid Rocket Engine*. Lulu.com.

[Pentagon Turbot, nd] Pentagon Turbot (n.d.). O-ring design. Accessed: April 15, 2025.

[Perez et al., 2022] Perez, J., Riccardi, M., Cohen, D., Gerwin, B., Lloyd, J., Michel, J., Rodriguez, A. T., Stelling, J., Young, L., Zhao, S., DeSpain, K., Ess, N., Guilak, J., Keogh, J., Koester, C., Landin, E., Neathery, R., Ramsey, C., Romanova, A., Shekar, P., Weissberg, J., Xu, C., and Yang, E. (2022). Titan 2 hybrid rocket engine documentation. Technical report, Rice University.

[Rossi, A, 2022] Rossi, A (2022). Case Study: Polycarbonate Blast Room for Rocket Testing.

[Sutton and Biblarz, 2017] Sutton, G. P. and Biblarz, O. (2017). *Rocket Propulsion Elements*. John Wiley and Sons Inc., 9th edition.

[Yang, 2015] Yang, P. (2015). Numerical study of cavitation within orifice flow. Master's thesis, Texas A&M University, College Station, TX. Submitted to the Office of Graduate and Professional Studies in partial fulfillment of the requirements for the degree of Master of Science in Mechanical Engineering.